LETTER

Aspm knockout ferret reveals an evolutionary mechanism governing cerebral cortical size

Matthew B. Johnson[1,2], Xingshen Sun[3,4,5,15], Andrew Kodani[1,2,15], Rebeca Borges-Monroy[1,2,15], Kelly M. Girskis[1,2], Steven C. Ryu[1,2], Peter P. Wang[1,2], Komal Patel[6], Dilenny M. Gonzalez[1,2], Yu Mi Woo[7], Ziying Yan[3,4,5], Bo Liang[3,4,5], Richard S. Smith[1,2], Manavi Chatterjee[6], Daniel Coman[8,9,10], Xenophon Papademetris[9,10,11], Lawrence H. Staib[10,11,12], Fahmeed Hyder[8,9,10,11], Joseph B. Mandeville[13], P. Ellen Grant[14], Kiho Im[14], Hojoong Kwak[7], John F. Engelhardt[3,4,5], Christopher A. Walsh[1,2]* & Byoung-Il Bae[1,2,6]*

The human cerebral cortex is distinguished by its large size and abundant gyrification, or folding. However, the evolutionary mechanisms that drive cortical size and structure are unknown. Although genes that are essential for cortical developmental expansion have been identified from the genetics of human primary microcephaly (a disorder associated with reduced brain size and intellectual disability)[1], studies of these genes in mice, which have a smooth cortex that is one thousand times smaller than the cortex of humans, have provided limited insight. Mutations in abnormal spindle-like microcephaly-associated (*ASPM*), the most common recessive microcephaly gene, reduce cortical volume by at least 50% in humans[2–4], but have little effect on the brains of mice[5–9]; this probably reflects evolutionarily divergent functions of *ASPM*[10,11]. Here we used genome editing to create a germline knockout of *Aspm* in the ferret (*Mustela putorius furo*), a species with a larger, gyrified cortex and greater neural progenitor cell diversity[12–14] than mice, and closer protein sequence homology to the human ASPM protein. *Aspm* knockout ferrets exhibit severe microcephaly (25–40% decreases in brain weight), reflecting reduced cortical surface area without significant change in cortical thickness, as has been found in human patients[3,4], suggesting that loss of 'cortical units' has occurred. The cortex of fetal *Aspm* knockout ferrets displays a very large premature displacement of ventricular radial glial cells to the outer subventricular zone, where many resemble outer radial glia, a subtype of neural progenitor cells that are essentially absent in mice and have been implicated in cerebral cortical expansion in primates[12–16]. These data suggest an evolutionary mechanism by which ASPM regulates cortical expansion by controlling the affinity of ventricular radial glial cells for the ventricular surface, thus modulating the ratio of ventricular radial glial cells, the most undifferentiated cell type, to outer radial glia, a more differentiated progenitor.

We injected 148 ferret zygotes with genome editing constructs that targeted *Aspm* exon 15, mutations in which cause severe microcephaly in humans[17], and recovered 11 kits born at full term, all carrying insertions or deletions in the targeted exon (Fig. 1a–d). We established three stable *Aspm* germline knockout ferret lines, which showed comparable phenotypes. Loss of ASPM protein was confirmed in embryonic fibroblasts (Fig. 1e).

Aspm knockout ferrets displayed robust microcephaly (Fig. 1f–i), with up to 40% reduced brain weight (Fig. 1n), but no change in body weight (Fig. 1p), closely modelling the effects of human mutations[2–4,17]. Magnetic resonance imaging[18] (MRI) showed that, similar to humans[4],

loss of cortical volume and surface area followed an anterior-to-posterior gradient, and the frontal cortex was affected the most (Fig. 1f–k and Extended Data Table 1). By contrast, the thickness of the cortex in knockout ferrets was preserved, similar to the cortex of human patients with mutations in *ASPM*[2–4], and the cytoarchitecture and lamination of neurons was also preserved (Fig. 1l, m, o and Extended Data Fig. 1). This phenotype is distinct from *Aspm* knockout mice, which show approximately 10% reduced brain weight, variable body weight reduction, variable cortical thinning, and no discernible change in cortical surface area[5–9] (Fig. 1q). Therefore, the *Aspm* loss-of-function phenotype is more similar in ferrets than in mice to the phenotype of human patients with mutations in *ASPM*.

To elucidate the developmental mechanism by which microcephaly occurs, we analysed *Aspm* knockout ferrets during cortical neurogenesis (Fig. 2a–o and Extended Data Figs. 2, 3), which begins around embryonic day 24 (E24) and continues for two weeks after birth, at E41. In the embryonic cortex of wild-type ferrets, undifferentiated ventricular radial glial cells (VRGs) divide symmetrically to expand the pool of VRGs or divide asymmetrically to produce two distinct, more differentiated progenitor subtypes, intermediate progenitors and outer radial glia (ORGs; Fig. 1a). ORGs are multipotent, proliferative, unipolar progenitors, which are abundant in the outer subventricular zone (OSVZ), that express molecular markers, which are also expressed by VRGs, including SOX2, PAX6 and vimentin (VIM); whereas intermediate progenitors are neuronally fated, multipolar transit amplifying cells that predominate in the inner subventricular zone (ISVZ) and express TBR2 (which is encoded by *Eomes*)[12–14,16]. All three neural progenitor cell (NPC) populations express the mitotic marker Ki-67 and produce neurons that migrate radially into the cortical plate[12–14,16,19]. The cortex of *Aspm*^{+/−} ferrets at E35 and postnatal day 0 (P0) displayed a ventricular zone that was densely packed with PAX6^{+} or SOX2^{+} VRGs, and a less-dense zone of Ki-67^{+} NPCs that expressed SOX2, TBR2 or both in the SVZ (Fig. 2d–g and Extended Data Figs. 2, 3). By contrast, the cortex of *Aspm* knockout ferrets contained overabundant Ki-67^{+} NPCs in the basal SVZ and intermediate zone (Fig. 2e, f), reminiscent of the positioning of ORGs that normally populate the OSVZ[12–14,20]. Discontinuous clusters of basal NPCs were accompanied by thinning of the ventricular zone, suggesting that precocious OSVZ progenitors were derived by premature withdrawal from the ventricular zone (Fig. 2d–f and Extended Data Figs. 2, 3). Displaced OSVZ progenitors were more abundant frontally and dorsally (Fig. 2a–c), matching the topography of cortical volume reduction in the adult (Fig. 1f–k).

[1]Division of Genetics and Genomics, Manton Center for Orphan Disease Research, Boston Children's Hospital, Harvard Medical School, Boston, MA, USA. [2]Howard Hughes Medical Institute, Boston Children's Hospital, Harvard Medical School, Boston, MA, USA. [3]Department of Anatomy and Cell Biology, Center for Gene Therapy, University of Iowa, Iowa City, IA, USA. [4]Center for Gene Therapy, University of Iowa, Iowa City, IA, USA. [5]National Ferret Resource and Research Center, University of Iowa, Iowa City, IA, USA. [6]Department of Neurosurgery, School of Medicine, Yale University, New Haven, CT, USA. [7]Department of Molecular Biology and Genetics, Cornell University, Ithaca, NY, USA. [8]Magnetic Resonance Research Center (MRRC), Yale University, New Haven, CT, USA. [9]Quantitative Neuroscience with Magnetic Resonance (QNMR) Core Center, Yale University, New Haven, CT, USA. [10]Department of Radiology & Biomedical Imaging, Yale University, New Haven, CT, USA. [11]Department of Biomedical Engineering, Yale University, New Haven, CT, USA. [12]Department of Electrical Engineering, Yale University, New Haven, CT, USA. [13]Athinoula A. Martinos Center for Biomedical Imaging, Department of Radiology, Massachusetts General Hospital, Charlestown, MA, USA. [14]Division of Newborn Medicine, Fetal Neonatal Neuroimaging and Developmental Science Center, Boston Children's Hospital, Harvard Medical School, Boston, MA, USA. [15]These authors contributed equally: Xingshen Sun, Andrew Kodani, Rebeca Borges-Monroy. *e-mail: christopher.walsh@childrens.harvard.edu; byoung-il.bae@yale.edu
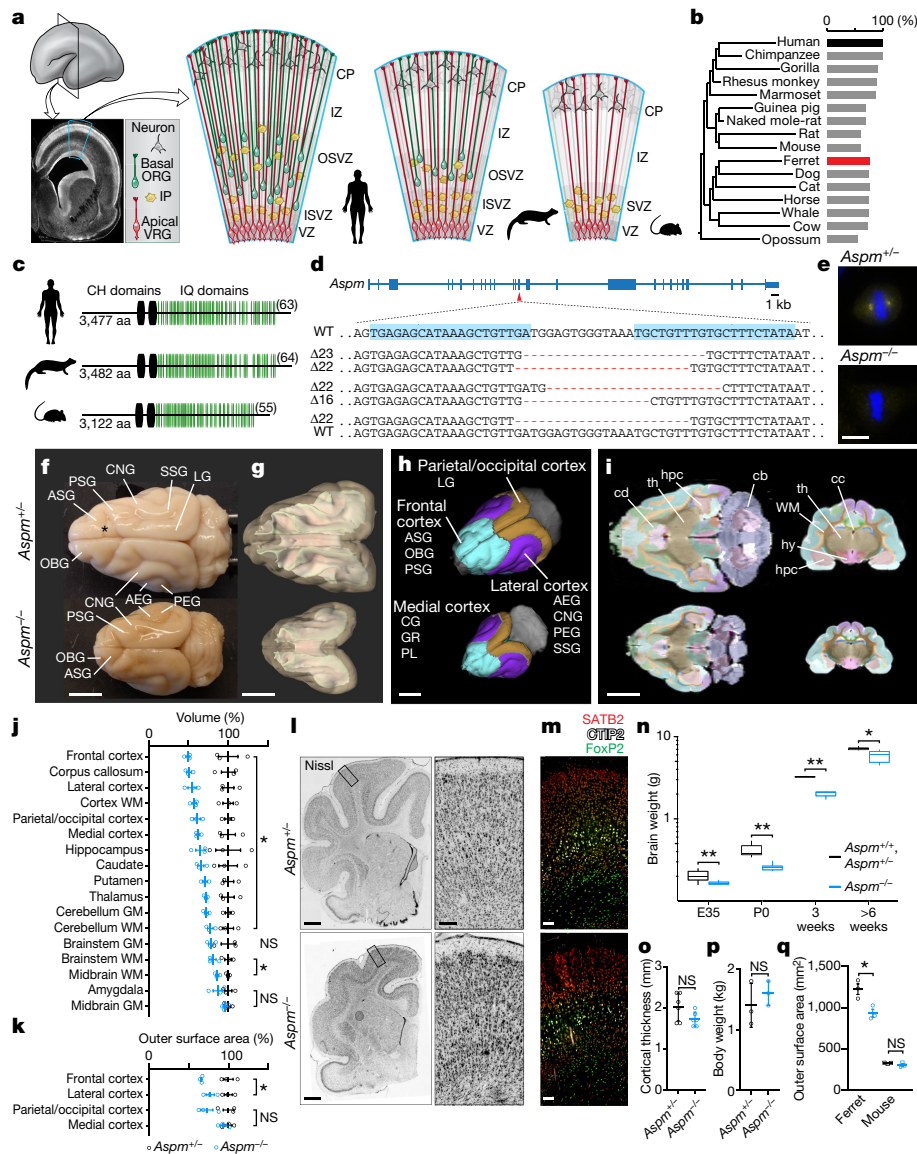
**Fig. 1 | *Aspm* knockout ferrets robustly model human microcephaly.**
a, NPC diversity in humans, ferrets and mice. **b, c**, ASPM protein is highly similar between humans and ferrets, including the number of calmodulin-binding (IQ) domains (**c**, in parentheses). **d**, Ferret *Aspm* gene showing the targeted sequences (blue highlights) and founder frameshift deletions. **e**, Loss of *Aspm* in knockout ferret embryonic fibroblasts. **f**, Brains of *Aspm*^{+/−} and *Aspm*^{−/−} ferret littermates. **g–k**, MRI segmentations of grey and white matter (**g**), gyri grouped into four regions (**h**), horizontal and coronal sections (**i**) and quantification of volume (**j**) and cortical surface area (**k**). *$P < 0.05$; $n = 3$ ferrets per genotype. **l–p**, *Aspm*^{−/−} ferrets show reduced brain weight (**n**, **$P < 0.005$; *$P < 0.01$; $n = 3$–17 ferrets per genotype per age group), but cytoarchitecture (**l**), laminar organization (**m**), cortical thickness (**o**, $n = 6$ ferrets per genotype) and body weight (**p**, $n = 3$ ferrets per genotype) are preserved. **q**, Loss of *Aspm* decreases

outer cortical surface area in ferrets, but not in mice ($n = 3$ ferrets and 3 mice per genotype). *$P = 0.0217$. Data are mean ± s.e.m. (**j, k, o–q**); box plots show maximum, third quartile, median, first quartile and minimum (**n**). See Methods, Extended Data Table 1 and Source Data for statistics and reproducibility. Scale bars, 10 μm (**e**), 100 μm (**m**), 1 mm (**l**) and 5 mm (**f–i**). AEG, anterior ectosylvian gyrus; ASG, anterior sigmoid gyrus; cb, cerebellum; cc, corpus callosum; cd, caudate; CG, cingulate gyrus; CH, calponin homology; CNG, coronal gyrus; CP, cortical plate; GR, gyrus rectus; GM, grey matter; hpc, hippocampus; hy, hypothalamus; IZ, intermediate zone; IP, intermediate progenitor; LG, lateral gyrus; OBG, orbital gyrus; PEG, posterior ectosylvian gyrus; PL, piriform lobe; PSG, posterior sigmoid gyrus; SSG, suprasylvian gyrus; th, thalamus; VZ, ventricular zone; WM, white matter.

Many displaced progenitors in the OSVZ of *Aspm* knockout ferrets expressed VRG/ORG markers including VIM, phosphorylated vimentin (pVIM), phosphorylated histone H3 (pH3), SOX2 and PAX6; as well as the ciliary marker ARL13B and the human ORG-enriched genes *Ptprz1* and *Hopx*[21], whereas other cells expressed the intermediate progenitor marker, as shown by TBR2 protein and *Eomes* mRNA analysis (Fig. 2g–o and Extended Data Figs. 2, 3, 6). Some of the displaced cells had an ORG-like unipolar morphology, with basal radial fibres that were immunoreactive to VIM, pVIM or HOPX antibodies (Fig. 2g–i, k, o). Quantification of pVIM[+] mitotic NPCs revealed a threefold increase in the number of ORG-like progenitors in the knockout ferrets at E35

($P = 0.006$; 3 *Aspm*^{+/−} and 4 *Aspm*^{−/−} littermates; Fig. 2j). The intermingled presence of NEUROG2^{+}HOPX[+] ORGs, TBR2^{+} intermediate progenitors and DCX^{+} newborn neurons together indicated preserved neurogenesis within clusters of displaced NPCs (Fig. 2n and Extended Data Fig. 6). These data demonstrate that the loss of *Aspm* in the ferret cortex causes VRGs to prematurely detach from the ventricular zone and relocate to the OSVZ, where many dislocated cells exhibit ORG morphology, molecular profile and neurogenic potential.

These marked changes in NPC populations in the knockout ferret contrast with six previously reported *Aspm* knockout mouse lines[5–9], which have consistently shown limited changes in NPC identity and
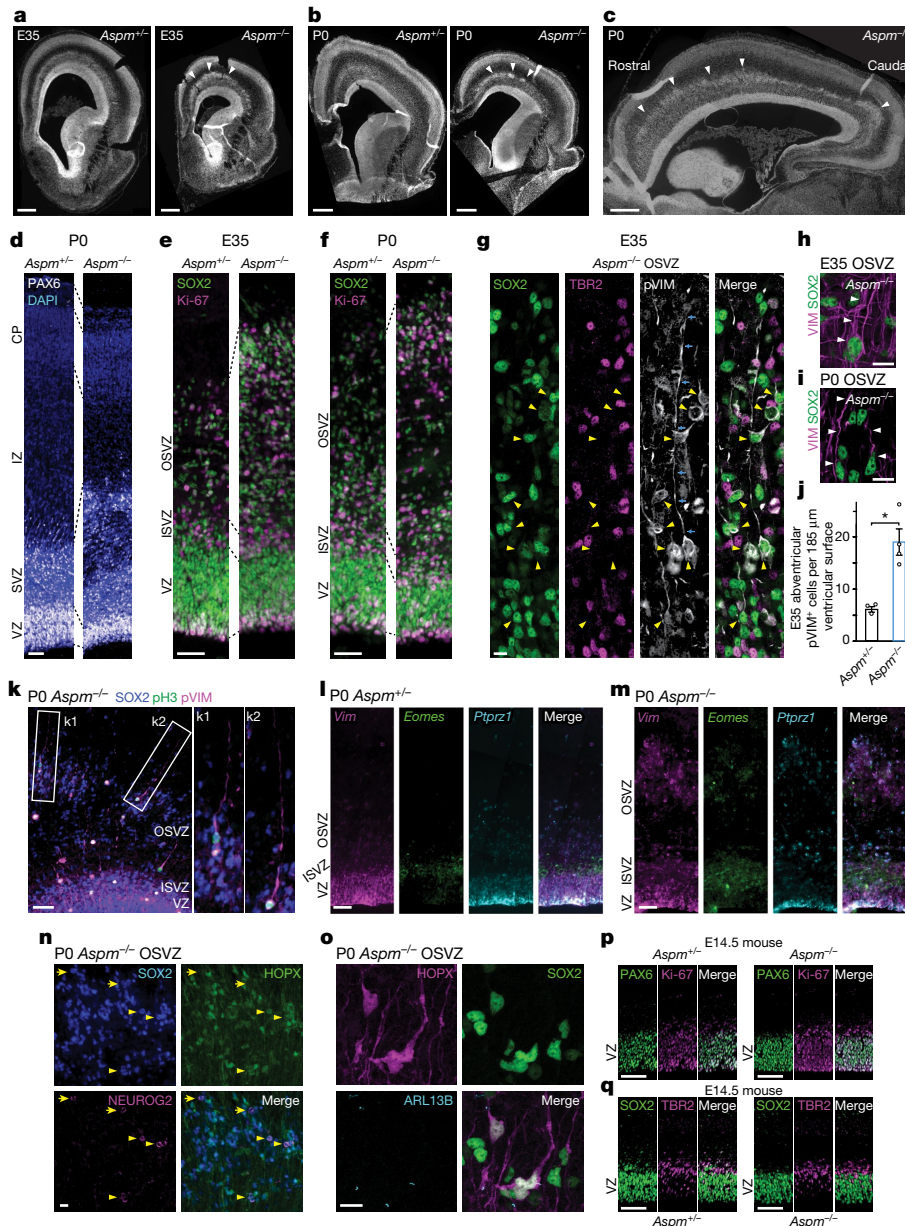
Fig. 2 | *Aspm* knockout ferrets show displaced NPCs. a–f, Nuclear staining of *Aspm*$^{-/-}$ ferret brains shows that there is a premature OSVZ-like zone (**a–c**, arrowheads), which contains NPCs that express PAX6, SOX2, and Ki-67 (**d–f**). **g–k**, Displaced NPCs include SOX2^{+}pVIM^{+} ORG (**g**, arrowheads) with a basal process (**g**, arrows; **h, i, k**) and TBR2^{+} intermediate progenitors. The number of abventricular pVIM^{+} NPCs are increased threefold in *Aspm*$^{-/-}$ ferrets (**j**). *$P = 0.006$; analysed using a one-tailed *t*-test; data are mean ± s.e.m.; $n = 3$ *Aspm*$^{+/-}$ and $n = 4$ *Aspm*$^{-/-}$ animals. **l–o**, Displaced NPCs express *Vim*, *Eomes* or *Ptprz1* (**l, m**), have ARL13B^{+} cilia (**o**) and are either SOX2^{+}NEUROG2^{+}HOPX^{+} (arrowheads) or SOX2^{+}NEUROG2^{+}HOPX^{-} (arrows) (**n**). **p, q**, *Aspm*$^{-/-}$ mice lack displaced NPCs. See Methods for statistics and reproducibility. Scale bars, 10 μm (**g–i, n, o**), 50 μm (**d–f**), 100 μm (**k–m, p, q**) and 500 μm (**a–c**).

organization. *Aspm* knockout mice show a trend towards an increased number of intermediate progenitors at the expense of VRGs[9], but lack ectopic basal SOX2^{+} or PAX6^{+} NPCs (Fig. 2p, q and Extended Data Fig. 4). *Aspm* knockout ferrets also showed increased cell apoptosis in telencephalic germinal zones that was not seen in *Aspm* knockout mice[5–7,9] (Extended Data Fig. 5), further highlighting that loss of *Aspm* elicits divergent brain phenotypes in ferrets and mice.

Single-cell RNA-sequencing[22] (scRNA-seq) of around 21,000 cells from the telencephalons of seven E35 embryos (3 *Aspm*$^{+/+}$ or *Aspm*$^{+/-}$ and 4 *Aspm*$^{-/-}$ animals) reinforced the conclusion that NPC proportions were altered in the *Aspm* knockout animals, although their transcriptional programs were mostly preserved (Fig. 3, Extended Data Fig. 7 and Extended Data Table 2). We identified cell clusters corresponding to excitatory and inhibitory progenitor and neuronal subtypes, as well as non-neural cells (Fig. 3a, b) and found that the

cell type composition of the E35 *Aspm* knockout forebrain was significantly altered ($\chi^2 = 267.27$, degrees of freedom $= 12$, $P = 2.2 \times 10^{-16}$), yet cells still clustered by cell type, not by genotype or batch (Extended Data Fig. 7). Consistent with immunohistochemical observations, scRNA-seq analysis suggested that VRGs, wild-type ORGs and prematurely displaced knockout ORGs were transcriptionally indistinguishable, and the total proportion of radial glial cells (cycling radial glial cells and interphase radial glial cells) was unchanged in *Aspm* knockout cells (Extended Data Table 2). A 30% increase in the proportion of intermediate progenitors in knockout ferrets ($P = 0.0002$, false discovery rate of < 0.01; Fig. 3c and Extended Data Table 2) was consistent with the increased number of intermediate progenitors that were detected by immunostaining (Fig. 2l, m and Extended Data Fig. 6) and was further validated by single-molecule fluorescence in situ hybridization (Fig. 3d, e). A doubling of the small proportion of
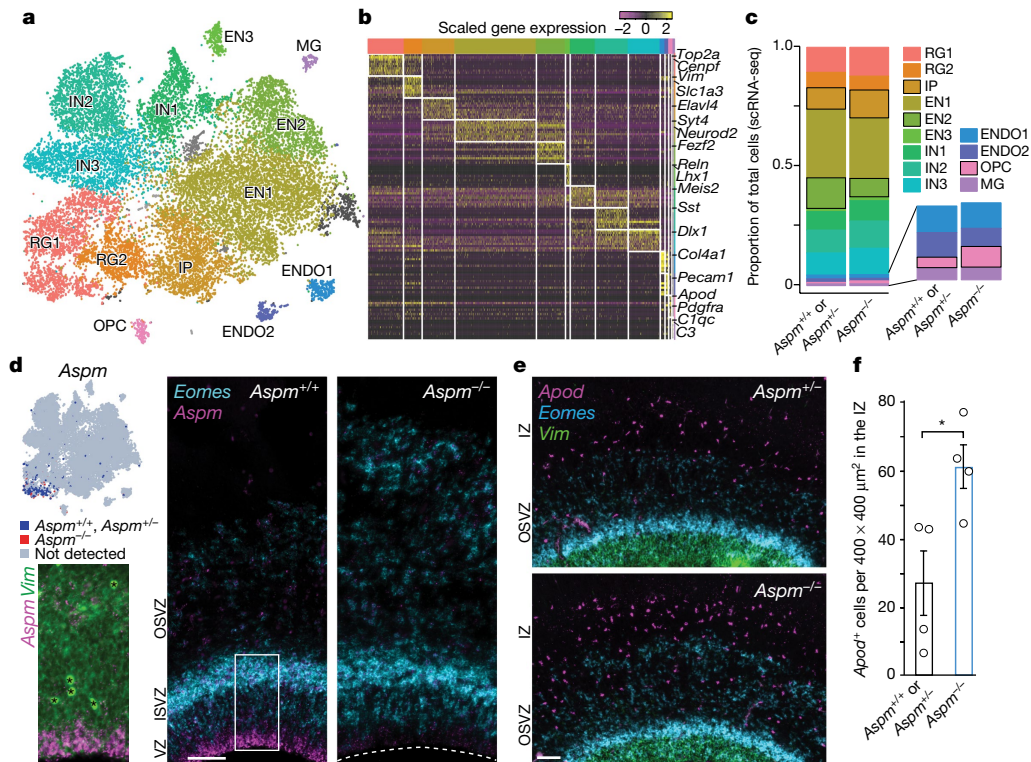
Fig. 3 | Loss of *Aspm* changes cell type proportions but not transcriptional programs. a, scRNA-seq identifies major cell types at E35. For abbreviations and statistics, see Extended Data Table 2. **b**, Cell type markers for each cluster. **c**, Proportions of each cell type, with the largest changes indicated by black outlines (bootstrap false discovery rate < 0.01). **d**, *Aspm* is enriched at the apical surface of the ventricular zone, whereas the number of *Eomes*[+] intermediate progenitors is increased in the SVZ of *Aspm* knockout ferrets. Asterisks indicate blood vessels. **e, f**, The number of *Apod*[+] oligodendrocyte precursor cells is increased in *Aspm*^{−/−} ferrets. *P = 0.012; analysed using a one-tailed *t*-test; *n* = 4 animals per genotype. See Methods for statistics and reproducibility. Data are mean ± s.e.m. Scale bars, 100 μm.

cells that expressed the oligodendrocyte precursor cell markers *Apod* and *Olig1* suggested limited but significant premature differentiation towards the glial lineage (Fig. 3c, e, f and Extended Data Table 2). These scRNA-seq data suggest that the gene expression programs of cortical neurogenesis are mostly preserved, but the proportions of developmental cell types are changed, in microcephaly associated with *ASPM* mutations.

While examining potential molecular mechanisms for the detachment of VRGs from the ventricular surface in the knockout ferret, we identified a novel interaction between ASPM, which is localized at the centrosome, and the apical polarity complex (Fig. 4). Together with other centrosomal proteins, ASPM is essential for normal stem cell behaviour, such as centriole biogenesis and maternal centriole structure (Extended Data Fig. 8), and interactions between the mother centriole and the apical membrane have been implicated in the maintenance of NPC stem cell character[9,23–25]. In VRGs, the centrosome is localized to the ventricular endfeet, which are linked by adherens junctions to form a polarized neuroepithelium, which expresses apical polarity complex proteins at the ventricular surface[26]. *Aspm*^{−/−} mice showed abrogated staining of the core apical complex protein aPKCζ along the disrupted ventricular surface at E14.5 (Fig. 4a). Intriguingly, we found that depletion of ASPM by RNA interference in H4 human neuroglioma cells resulted in the loss of PKCζ and another critical apical complex protein, PAR6α, from the centrosome (Fig. 4b). Furthermore, we found an interaction between ASPM and PKCζ, as indicated by mutual co-immunoprecipitation (Fig. 4c), that may mediate centrosomal recruitment of the apical polarity complex, providing a new mechanistic insight into the link between centrosomal microcephaly-related proteins and apical progenitor identity.

Finally, we found sharply reduced staining for ninein, another microcephaly-associated centrosomal protein[27], at both the E14.5 mouse and E35 ferret ventricular surface (Fig. 4d, e). Ninein localizes

to the mother centriole and is critical for NPC maintenance[25,28], and depletion of either ASPM or PKCζ in H4 cells reduced centrosomal localization of ninein (Fig. 4f). Importantly, *Aspm*^{−/−} mouse embryonic fibroblasts expressed normal levels of aPKCζ, PAR6, and ninein proteins, suggesting that loss of aPKCζ and ninein from the ventricular surface of *Aspm* knockout mice and ferrets is primarily because of mislocalization, rather than downregulation. These data show that loss of ASPM disturbs the organization and function of the centrosome at multiple levels, and suggest disruption of the centrosome–apical polarity complex interface as a mechanism underlying the displacement of VRGs from the ventricular zone in the *Aspm* knockout ferret.

Collectively, our data show that ASPM regulates the affinity of VRGs for the ventricular surface. Displaced mutant progenitors show many features of ORGs, indicating that ASPM has a central role in the regulation of the normal timing of the transition from VRG to ORG, and thus the ratio of VRGs to ORGs over the course of development. Premature basal displacement deprives VRGs of proliferation-inducing factors obtained from the cerebrospinal fluid[29], increases the proportions of less-proliferative ORGs and intermediate progenitors, and results in a smaller cerebral cortex. The frontal predominance that characterizes both the loss of cortical surface area and VRG displacement further indicates that the premature transformation of VRG to ORG leads directly to reduced cortical units and surface area.

Our results support the idea that expansion of cortical surface area during human evolution may have arisen in part from changes to the proliferative time window of VRGs. Changes in the amino acid sequence of ASPM and other microcephaly-associated centrosomal proteins[10] may have affected the timing of the VRG proliferative window by altering interactions between maternal centriole components and the apical polarity complex. Finally, we find that for human brain disorders that are poorly recapitulated in the mouse or in cell culture, the ferret is an efficient and accurate genetic model that demonstrates
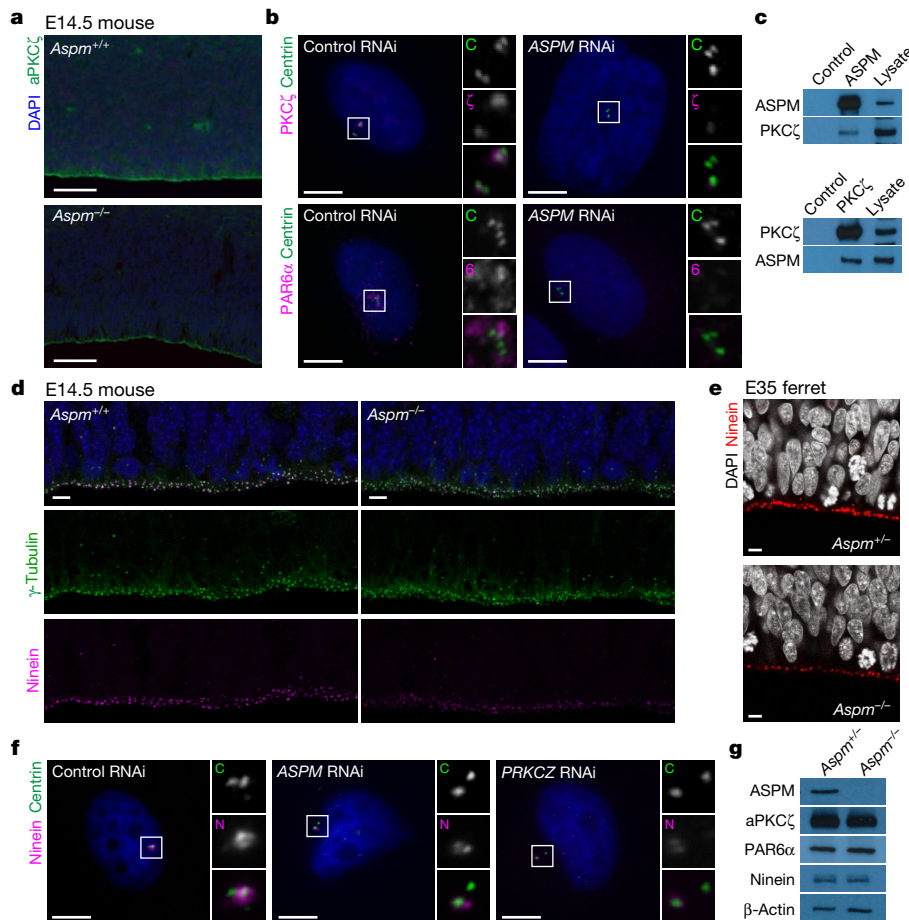
Fig. 4 | ASPM controls localization of apical polarity complex proteins to the centrosome. a, aPKCζ at the ventricular surface is decreased in *Aspm⁻/⁻* mice. **b,** Depletion of ASPM in H4 cells prevents recruitment of PKCζ and PAR6α to the centrosomes. RNAi, RNA interference. **c,** ASPM and PKCζ co-immunoprecipitate in extracts of HeLa cells. **d, e,** Loss of ASPM decreases ventricular surface staining for ninein in mice (**d**) and ferrets (**e**). **f,** Depletion of ASPM and PKCζ prevents recruitment of ninein to the centrosomes in H4 cells. **g,** Levels of aPKCζ, PAR6α, and ninein are unchanged in *Aspm⁻/⁻* mouse embryonic fibroblasts. See Methods for reproducibility. For gel source data, see Supplementary Data. Scale bars, 5 μm (**b, d-f**) and 50 μm (**a**).

robust phenotypes and can be used to investigate the mechanisms underlying disorders of the brain.

Online content

Any Methods, including any statements of data availability and Nature Research reporting summaries, along with any additional references and Source Data files, are available in the online version of the paper at https://doi.org/10.1038/s41586-018-0035-0.

1. Faheem, M. et al. Molecular genetics of human primary microcephaly: an overview. *BMC Med. Genomics* **8**, S4 (2015).
2. Bond, J. et al. *ASPM* is a major determinant of cerebral cortical size. *Nat. Genet.* **32**, 316–320 (2002).
3. Passemard, S. et al. Abnormal spindle-like microcephaly-associated (*ASPM*) mutations strongly disrupt neocortical structure but spare the hippocampus and long-term memory. *Cortex* **74**, 158–176 (2016).
4. Desir, J., Cassart, M., David, P., Van Bogaert, P. & Abramowicz, M. Primary microcephaly with ASPM mutation shows simplified cortical gyration with antero-posterior gradient pre- and post-natally. *Am. J. Med. Genet. A* **146A**, 1439–1443 (2008).
5. Pulvers, J. N. et al. Mutations in mouse *Aspm* (abnormal spindle-like microcephaly associated) cause not only microcephaly but also major defects in the germline. *Proc. Natl Acad. Sci. USA* **107**, 16595–16600 (2010).
6. Fujimori, A. et al. Disruption of *Aspm* causes microcephaly with abnormal neuronal differentiation. *Brain Dev.* **36**, 661–669 (2014).
7. Capecchi, M. R. & Pozner, A. ASPM regulates symmetric stem cell division by tuning cyclin E ubiquitination. *Nat. Commun.* **6**, 8763 (2015).
8. Williams, S. E. et al. Aspm sustains postnatal cerebellar neurogenesis and medulloblastoma growth in mice. *Development* **142**, 3921–3932 (2015).
9. Jayaraman, D. et al. Microcephaly proteins Wdr62 and Aspm define a mother centriole complex regulating centriole biogenesis, apical complex, and cell fate. *Neuron* **92**, 813–828 (2016).
10. Montgomery, S. H. & Mundy, N. I. Microcephaly genes evolved adaptively throughout the evolution of eutherian mammals. *BMC Evol. Biol.* **14**, 120 (2014).
11. Bae, B. I., Jayaraman, D. & Walsh, C. A. Genetic changes shaping the human brain. *Dev. Cell* **32**, 423–434 (2015).
12. Fietz, S. A. et al. OSVZ progenitors of human and ferret neocortex are epithelial-like and expand by integrin signaling. *Nat. Neurosci.* **13**, 690–699 (2010).
13. Reillo, I., de Juan Romero, C., García-Cabezas, M. A. & Borrell, V. A role for intermediate radial glia in the tangential expansion of the mammalian cerebral cortex. *Cereb. Cortex* **21**, 1674–1694 (2011).
14. Johnson, M. B. et al. Single-cell analysis reveals transcriptional heterogeneity of neural progenitors in human cortex. *Nat. Neurosci.* **18**, 637–646 (2015).
15. Smart, I. H., Dehay, C., Giroud, P., Berland, M. & Kennedy, H. Unique morphological features of the proliferative zones and postmitotic compartments of the neural epithelium giving rise to striate and extrastriate cortex in the monkey. *Cereb. Cortex* **12**, 37–53 (2002).
16. Hansen, D. V., Lui, J. H., Parker, P. R. & Kriegstein, A. R. Neurogenic radial glia in the outer subventricular zone of human neocortex. *Nature* **464**, 554–561 (2010).
17. Bond, J. et al. Protein-truncating mutations in *ASPM* cause variable reduction in brain size. *Am. J. Hum. Genet.* **73**, 1170–1177 (2003).
18. Hutchinson, E. B. et al. Population based MRI and DTI templates of the adult ferret brain and tools for voxelwise analysis. *Neuroimage* **152**, 575–589 (2017).
19. Martínez-Cerdeño, V. et al. Comparative analysis of the subventricular zone in rat, ferret and macaque: evidence for an outer subventricular zone in rodents. *PLoS ONE* **7**, e30178 (2012).
20. Martínez-Martínez, M. A. et al. A restricted period for formation of outer subventricular zone defined by Cdh1 and Trnp1 levels. *Nat. Commun.* **7**, 11812 (2016).
21. Pollen, A. A. et al. Molecular identity of human outer radial glia during cortical development. *Cell* **163**, 55–67 (2015).

22. Macosko, E. Z. et al. Highly parallel genome-wide expression profiling of individual cells using nanoliter droplets. *Cell* **161**, 1202–1214 (2015).
23. Kodani, A. et al. Centriolar satellites assemble centrosomal microcephaly proteins to recruit CDK2 and promote centriole duplication. *eLife* **4**, e07519 (2015).
24. Paridaen, J. T., Wilsch-Bräuninger, M. & Huttner, W. B. Asymmetric inheritance of centrosome-associated primary cilium membrane directs ciliogenesis after cell division. *Cell* **155**, 333–344 (2013).
25. Wang, X. et al. Asymmetric centrosome inheritance maintains neural progenitors in the neocortex. *Nature* **461**, 947–955 (2009).
26. Singh, S. & Solecki, D. J. Polarity transitions during neurogenesis and germinal zone exit in the developing central nervous system. *Front. Cell. Neurosci.* **9**, 62 (2015).
27. Dauber, A. et al. Novel microcephalic primordial dwarfism disorder associated with variants in the centrosomal protein ninein. *J. Clin. Endocrinol. Metab.* **97**, E2140–E2151 (2012).
28. Zhang, X. et al. Cell-type-specific alternative splicing governs cell fate in the developing cerebral cortex. *Cell* **166**, 1147–1162 (2016).
29. Lehtinen, M. K. et al. The cerebrospinal fluid provides a proliferative niche for neural progenitor cells. *Neuron* **69**, 893–905 (2011).

METHODS

We complied with all relevant ethical regulations and the experiments that we performed were approved by the Institutional Animal Care and Use Committees (IACUCs) at the University of Iowa, Boston Children's Hospital, Yale School of Medicine and Marshall BioResources.

ASPM protein homology and domain analysis. ASPM protein sequences of 16 mammals were extracted from NCBI GenBank. Global pairwise alignment was performed with EMBOSS Needleall (http://www.ebi.ac.uk/Tools/psa/emboss_needle/). The percentage of homology to human ASPM was calculated for each animal based on the alignment score using the Needleman–Wunsch algorithm (gap opening penalty, 10; gap extension penalty, 0.5). The phylogenetic tree was generated using http://timetree.org. CH and IQ domains were counted using the simple modular architecture research tool (http://smart.embl.de/), for NP_060606.3 (human), NP_033921.3 (mouse) and ENSMPUT00000010205.1 (ferret).

TALEN assembly and mRNA synthesis. We assembled three pairs of transcription activator-like effector nucleases (TALENs) that target exon 15 of ferret *Aspm*, which encodes the second CH domain, and cloned the TALENs into a mammalian expression vector with CMV and T7 promoters through a commercial service (PNA Bio). Gene targeting efficiency of each TALEN pair was tested in HEK293T cells using a split GFP-based reporter[30]. The most efficient pair, targeting TGAGAGCATAAAGCTGTTGATGGAGTGGGTAAA TGCTGTTTGTGCTTTCTATA (target–spacer–target) was chosen for genome editing *in vivo*. These plasmids are available from Addgene. For mRNA synthesis, endotoxin-free TALEN plasmids were prepared using NucleoBond Xtra Midi EF kit (Clontech), ethanol-precipitated three times, linearized using ScaI digestion (New England BioLabs) and gel-purified. mRNAs were synthesized using the mMessage mMachine T7 ULTRA kit (ThermoFisher Scientific) and cleaned up using the MEGAclear transcription clean-up kit (ThermoFisher Scientific). Of note, we performed the optional ammonium acetate precipitation to improve the quality of the mRNAs. The TALEN mRNAs were diluted in sterile EmbryoMax injection buffer (Millipore) at 50 ngμl^{-1}, aliquoted and kept frozen at $-150\,°C$ until use.

Embryonic targeting of the ferret *Aspm* gene. Zygotes were collected from the mating of ferrets with a sable coat colour (Marshall BioResources) as previously described[31]. TALEN mRNA (50 ngμl^{-1}) was injected into the cytoplasm of zygotes using a micromanipulator and injector (Eppendorf) and a phase-contrast microscope. Initially 79 ferret zygotes were injected and cultured in vitro for five days so that they reached the blastocyst stage. Twelve zygotes developed to blastocysts, from each of these zygotes genomic DNA was extracted and whole-genome multiple displacement amplification was performed. The targeted genomic region was amplified by PCR (primers: 5′-TTTGTGTGTGTTTCAGGTGGA-3′ and 5′-TGCATTATACAACTGGTGACAGA-3′ with a 430-bp product size), gel-purified and cloned using a TOPO-TA cloning kit (ThermoFisher Scientific). Twelve plasmid clones were sequenced from individual bacterial colonies from each blastocyst. These studies demonstrated an 87% targeting efficiency (14 insertions or deletions in 16 alleles or 8 blastocysts that we were able to analysis). Next, we injected 148 zygotes, incubated them at 39 °C for 24 h, and transferred 116 two-cell-stage embryos into the oviduct of pseudopregnant female sable ferrets as previously described[31]. Twenty-three ferrets were born and eleven survived. All 11 ferrets had insertions or deletions (100% efficiency). The F_0 ferrets suckled and swallowed milk normally and grew without gross abnormalities.

Germline transmission. Six *Aspm* mutant ferrets were shipped to Marshall BioResources at three months of age and maintained according to the protocol approved by IACUC. Two compound heterozygous males, $\Delta23;\Delta22$ (c.3364_3386del;c.3363_3384del) and $\Delta22;\Delta16$ (c.3367_3388del;c.3364_3379 del), and one heterozygous female, $\Delta22;WT$ (c.3363_3384del;WT), (Fig. 1d) were chosen as founders, because they had similar frameshift, early truncating mutations. They were bred to each other or wild-type ferrets. Germline transmission was confirmed by T7 endonuclease I assay (New England BioLabs) and sequencing of both alleles. Eventually animals with a specific $\Delta22$ mutation (c.3363_3384del) were maintained for breeding. Routine genotyping was carried out with PCR (primers: 5′-ATCAATAAGAAAAAAGACAAAAGAAATAGTGG-3′ and 5′-CTTAAGTCAGTGAGCTTAAACAGAAAT-3′ with a 150-bp product size for the wild-type allele and 128-bp from the knockout allele). *Aspm* knockout males mated successfully, and knockout kits were born at expected Mendelian ratios.

Semen analysis. Every mating was closely monitored at Marshall BioResources. Sperm samples were collected from mated females directly after mating. The concentration, motility and morphology of the sperm were analysed by an experienced technician. Each male received a sperm check evaluation at least once a month. Samples from $Aspm^{+/+}$, $Aspm^{+/-}$ and $Aspm^{-/-}$ males showed similar sperm counts.

Ferret colony management and tissue handling. The *Aspm* knockout ferret colony was maintained at Marshall BioResources. For embryonic ages and < P8, timed pregnant jills were shipped to Boston Children's Hospital and euthanized before embryo extraction, at which point brains were removed from the embryos and drop-fixed in 4% paraformaldehyde (PFA) at 4 °C overnight. For $\geq$P8 ferrets, all animals were deeply anaesthetized and weighed before transcardial perfusion with cold PBS followed by 4% PFA, after which the brains were extracted and placed in 4% PFA at 4 °C overnight. The brains were subsequently washed and stored in PBS before processing for immunohistochemistry. All brain weight measurements were made post-fixation, before sucrose infiltration.

MRI. *Ferrets.* Three $Aspm^{+/-}$ and three $Aspm^{-/-}$ ferrets (>8 months of age) were perfused using 4% PFA in PBS. The brains were dissected and post-fixed in PFA and PBS containing 4 mM gadolinium contrast Magnevist (Bayer) at 4 °C for two weeks. The brains were scanned using a 9.4 T at Yale Magnetic Resonance Center and the Martinos Center for Biomedical Imaging, Massachusetts General Hospital. At Yale, a custom-made ^{1}H radiofrequency coil (40-mm diameter) was used for diffusion tensor imaging (DTI). DTI acquisition was obtained with a Stejskal and Tanner spin-echo diffusion-weighted sequence with a diffusion gradient $\delta = 5$ ms and a delay $\Delta = 15$ ms between diffusion gradients[32]. Sixty-four slices of 500-μm thickness, field of view of 25.6×25.6 mm^2 and 128×128 resolution were acquired with a repetition time (TR) of 4 s, echo time (TE) of 30 ms and four averages. Each of the six MR images was first corrected for B1 shading artefacts using a slice inhomogeneity correction[33] and an inverse covariance mapping of grey matter density (D.C., X.P., L.H.S & F.H., unpublished observations). Next, the Ferret Atlas[18] was registered to each of the MRI images using a tensor *b*-spline normalized mutual information nonlinear intensity-based registration algorithm[34,35] with a control point spacing of 1 mm. The result of the registration was used to warp the atlas regions to each individual MRI, and from this we calculated the volume of each of the warped regions as shown in Fig. 1 and Extended Data Table 1. Anterior sigmoid gyrus, orbital gyrus and posterior sigmoid gyrus were considered to be frontal cortex; anterior ectosylvian gyrus, coronal gyrus, posterior ectosylvian gyrus, and suprasylvian gyrus were considered to be lateral cortex; cingulate gyrus, gyrus rectus and piriform lobe were considered to be medical cortex; and lateral gyrus was considered to be the parietal/occipital cortex. The name of each brain part in Fig. 1 is as previously described[36]. For DTI tensor measurement, a total of 15 different non-collinear diffusion weighted directions ($b = 1{,}000$ s mm^{-2}) and 1 without diffusion weighting were obtained. The six elements of the diffusion tensor were calculated from the signal intensity of the diffusion-weighed images. Tensor eigenvalues and their corresponding eigenvectors were computed, along with fractional anisotropy, at each voxel. The images were colour-coded by the principal direction (eigenvector) of diffusion using BioImage Suite[37] (http://www.bioimage-suite.org/). At Massachusetts General Hospital, we acquired anatomically accurate brain volume images with minimal distortion using FLASH (fast low angle shot) MRI sequence with TR $= 100$ ms, TE $= 30$ ms and 150-μm isotropic resolution. Cortical grey and white matter were manually segmented using FreeView (http://surfer.nmr.mgh.harvard.edu) and their volumes were measured.

Mice. Three $Aspm^{+/+}$ and three $Aspm^{-/-}$ mouse brains were dissected from P30 animals perfused with 4% PFA and post-fixed as described above. Brains were submerged into perfluorocarbon oil (Fomblin, Fisher Scientific) at 4 °C for three days, and imaged in this oil using a Bruker BioSpec 70/30 7 T MRI scanner (a sub-millimetre MRI with a 30-cm bore and 450 mT m^{-1} gradient) in the Small Animal Imaging Facility at Boston Children's Hospital. MRI scans were isotropic 63-μm voxels across the entire brain. Cortical surface area was visualized and measured using the FreeView, Osyrix and ImageJ 3D projection.

Fluorescent immunohistochemistry. Fixed ferret brains were infiltrated with a series of 10%, then 20% and finally 30% w/v sucrose solutions in PBS until sunk, then embedded in optimal cutting temperature (OCT) compound and frozen in isopentane cooled to $-40\,°C$, after which they were stored long-term at $-80\,°C$. Brains were sectioned at 10- to 20-μm thickness on a Leica Cryostat, mounted immediately onto warm charged SuperFrost Plus slides (Fisher Scientific) and dried at 37 °C for 10 to 30 min before storage at $-80\,°C$. After applying a hydrophobic barrier around the tissue (ImmEdge Pen, Vector Labs), slides were washed in cold 0.1 M PBS followed by antigen retrieval in Retrievagen A pH 6.0 (BD Biosciences) at 80–90 °C in a hybridization oven for 45 min. Sections were then cooled to room temperature in Retrievagen, washed in cold 0.1 M PBS, and blocked for 1 h at room temperature (5% normal donkey serum, 1% w/v BSA, 0.2% w/v glycine and 0.2% w/v lysine, in PBS). Slides were incubated with primary antibodies for two nights on a rotary shaker at 4 °C in blocking buffer plus 0.3% Triton X-100. Sections were then washed in PBS and incubated for 2 h at room temperature in blocking buffer containing secondary antibodies at 1:500 (Jackson Immunoresearch). Finally, slides were washed in PBS, counterstained with DAPI at 1 μg ml^{-1} in PBS for 15 min, washed again and coverslipped with Fluoromount-G (Southern Biotech). Images were obtained with a Zeiss LSM700 confocal microscope and Leica MZ16 F fluorescence stereomicroscope. The following antibodies were used at 1:200–1:2,000: PAX6 (Abcam ab5790), FoxP2 (Abcam ab16046), CTIP2 (Abcam ab18465), SATB2 (Bethyl A301-864A), SATB2 (Abcam ab51502), SOX2 (SCBT sc-17320), TBR2 (Millipore AB15894), Ki-67 (BD 550609), pVIM (MBL D076-3), VIM (Abcam

ab8978), pH3 (Millipore 07-145), HOPX (SCBT sc-30216), ARL13B (Abcam ab136648), ARL13B (ProteinTech 17711-1-AP), NEUROG2 (R&D MAB3314) and DCX (SCBT sc-8066).

Apoptosis assay. We examined apoptosis on cryosections using the ApopTag Red In situ Apoptosis Detection Kit (Millipore) according to the manufacturer's protocol.

scRNA-seq. *Cell capture and sequencing.* Cell capture and sequencing were performed using the Drop-seq method[22] (http://mccarrolllab.com/dropseq/). Forebrain tissue was isolated from 2 $Aspm^{+/+}$, 1 $Aspm^{+/-}$ and 4 $Aspm^{-/-}$ E35 ferret embryos and cryopreserved[38], then shipped to Cornell and processed there for single-cell capture, library preparation and sequencing.

Read alignment and digital gene expression matrix generation. Ferret reference gene annotations were expanded using bulk RNA-seq data from the cortex of two P2 ferrets. Bulk data were first mapped to the Ensembl ferret reference genome and transcriptome using TopHat2, and a transcriptome was assembled with cufflinks; this assembled transcriptome and the Ensembl reference transcriptome version 1.0.85 were merged using cuffmerge[39]. The Drop-Seq Core Computational Protocol version 1.0.1 was followed[22]. Fastq reads were converted to BAM using the 'FastqToSam' command in Picard (http://broadinstitute.github.io/picard/). Read pairs for which more than one base in the barcode had a quality below 10 were discarded. Adaptor sequences were trimmed from the 5′ end of the read, along with polyA tails. Star-2.5.2a[40] was used to map reads to the custom transcriptome reference. The digital gene expression matrix was extracted using the 'DigitalExpression' program of the Drop-seq protocol[22], keeping only cells with at least 200 reads per cell for clustering analysis.

Single cell clustering. Seurat software was used for dimensionality reduction, clustering and obtaining cluster markers[41]. Cells from $Aspm^{+/+}$ or $Aspm^{+/-}$ and $Aspm^{-/-}$ ferrets were merged in a single matrix. An initial run showed that one of the $Aspm^{+/-}$ samples contained low Unique Molecular Identifier (UMI) and gene counts compared to the other samples, and clustered differently, so this sample was removed from downstream analyses (Extended Data Fig. 7). Genes were included if they were expressed in ≥3 cells and cells were included if they expressed > 200 genes and < 2,000 genes. This resulted in 22,211 cells and 21,962 genes from 8,037 $Aspm^{+/+}$ or $Aspm^{+/-}$ cells and 14,174 $Aspm^{-/-}$ cells. The data were log-normalized per cell, scaling each cell to 10,000 molecules as described previously[22]. The 'MeanVarPlot' Seurat function was used to identify the most variable genes, obtaining 3,555 variable genes. Negative binomial regression was performed on the variable genes, using the number of UMIs per cell as a confounder variable before clustering. The 'PCAFast' function in Seurat was used to implement principal component analysis using the IRLBA package. Twenty-five principal components were selected for clustering and as input for t-distributed stochastic neighbour embedding (t-SNE) in Seurat. These were selected by plotting the standard deviation of the principal components and setting a cutoff at the 'elbow' of the graph using the 'PCElbowPlot' function in Seurat. Clustering was performed using the Seurat function 'FindClusters', which implements a shared nearest neighbour modularity optimization based algorithm using k.param = 30 for defining the k of the k-nearest neighbour algorithm and a resolution of 0.5 as previously described[41,42]. The Barnes–Hut implementation of t-SNE was used for visualizing the clusters using the 'RunTSNE' and 'TSNEPlot' Seurat functions. We observed a co-localization in the t-SNE plot of cells clustered together by the graph-based clustering algorithm (Fig. 3a). Cluster markers were obtained with the 'FindAllMarkers' Seurat function using a likelihood-ratio test, using the parameter min.pct = 0.25 to test only genes expressed in at least 25% of cells in either all cells or the cells in a specific cluster, and testing only genes with at least 0.25-fold difference on a log-scale between cells in a cluster and all cells using the parameter thresh.use = 0.25. P values were adjusted for multiple-comparison testing using the p.adjust function in R for the Benjamini–Hochberg false discovery rate (FDR), selecting an FDR threshold of 0.01. Known markers were used to determine the corresponding cell type of each cluster. The heat map in Fig. 3b shows expression data for the top ten cluster markers for each cluster, in a random sample of 10% of the cells of each cluster. Plotting cells onto the t-SNE plot based on their batch (three batches with $Aspm^{+/+}$ or $Aspm^{+/-}$ as well as $Aspm^{-/-}$ animals each) suggested that batches did not strongly influence clustering (Extended Data Fig. 7). Plotting cells from each sample onto the t-SNE plot suggested that two non-neuronal clusters of blood and choroid plexus epithelial cells were primarily from a single sample (a likely dissection artefact) and these two clusters were removed from further analysis (grey clusters in Fig. 3a and Extended Data Fig. 7c, d). Plotting the number of genes and UMIs in each cluster revealed that one of the excitatory neuronal clusters had almost three times as many genes and UMIs per cell (Extended Data Fig. 7c, d). This, along with the fact that this cluster expressed a combination of markers from the other two excitatory neuronal clusters suggested that this cluster may contain doublets or other technical or batch artefacts; therefore we also removed this cluster from further analysis.

Statistical analysis of cell type composition by genotype. A χ^2 test was performed using the 'chisq.test' function in R to test the association of cluster composition with

genotype. We also quantified the fraction of cells corresponding to each cluster with the assumption that Drop-seq captures and sequences cells in an unbiased manner, and that the frequencies of cells are representative of their frequency in the tissue[22]. The fraction of cells corresponding to each cluster was obtained by counting the number of cells assigned to each cluster for $Aspm^{+/+}$ or $Aspm^{+/-}$ and $Aspm^{-/-}$ samples and dividing over the total number of cells that passed the filters described above and excluding the three clusters that were removed, for a total of 7,645 $Aspm^{+/+}$ and $Aspm^{+/-}$ cells and 13,725 $Aspm^{-/-}$ cells. Empirical P values were obtained by permuting a genotype 10,000 times and obtaining the fraction of cells corresponding to each cluster for each permutation. These fractions were sorted and the P value was obtained by counting the number of times a fraction was more extreme or equal to the observed fraction in the non-permuted data divided by 10,000 and multiplied by 2 for a two-tailed test. P values were adjusted for multiple comparison testing using the p.adjust function in R for the Benjamini–Hochberg FDR, selecting an FDR threshold of 0.01.

Single-molecule fluorescence in situ hybridization. Using RNAscope fluorescence detection assays and probes (ACDbio), we performed single-molecule fluorescence in situ hybridization according to the manufacturer's protocols. Cryosections on SuperFrost Plus slides (Fisher Scientific) were dried at −20 °C, rather than at room temperature or 37 °C, for 15 min after mounting, and were used within a week of sectioning. Target retrieval was performed at 80 °C in a hybridization oven for 30–40 min before proceeding with the RNAscope multiplex fluorescence detection protocol.

Cell culture and siRNA transfection. H4 and HeLa cells authenticated by short tandem-repeat profiling were obtained from ATCC, cultured in Advanced DMEM (ThermoFisher Scientific) supplemented with 3% FBS (Altantis) and Glutamax-I (ThermoFisher Scientific), and used within five passages with routine mycoplasma screening. Ferret embryonic fibroblasts (FEFs) and mouse embryonic fibroblasts (MEFs) were derived from post-fertilization day 35 and 14.5 embryos, respectively. FEFs and MEFs were cultured in AmnioMAX (ThermoFisher Scientific). H4 cells were transfected with validated siRNAs against human *ASPM* or *PRKCZ*, which encodes PKCζ (ThermoFisher Scientific), using Oligofectamine and OptiMEM (ThermoFisher Scientific) according to the manufacturer's instructions and were analysed 48 h later.

Immunoprecipitation and immunoblotting. Immunoprecipitation experiments were performed as previously described[9]. In brief, HeLa cells were collected in Dulbecco's PBS (DPBS, ThermoFisher Scientific) and lysed in lysis buffer (50 mM Tris-HCl pH 7.4, 266 mM NaCl, 2.27 mM KCl, 1.25 mM KH$_2$PO$_4$, 6.8 mM Na$_2$HPO$_4$-7H$_2$O and 1% NP-40) supplemented with EDTA-free protease inhibitors cocktail set III (Calbiochem). For each immunoprecipitation, 1 mg of lysate was incubated with 2 μg of antibody for 2 h and then incubated with magnetic protein G–sepharose beads (GE Healthcare Life Sciences) for another 1 h at 4 °C. Complexes were washed and then boiled in 2× Laemmli reducing buffer with β-mercaptoethanol (Bio-Rad). Samples were separated on 4–15% TGX gels (Bio-Rad), transferred onto BA85-supported nitrocellulose (GE Healthcare Life Sciences) at 100 V for 30–45 min using a plate electrode Trans-Blot cell with cooling coil (Bio-Rad) and then subjected to immunoblot analysis using ECL Lightening Plus (Perkin-Elmers) or Western Pico (ThermoFisher Scientific). All immunoprecipitation and immunoblotting experiments were replicated three times.

Fluorescent immunocytochemistry. Cells were fixed in ice-cold methanol for 3 min, permeabilized in blocking buffer (2.5% BSA or FBS, 0.1% Triton X-100, 0.03% NaN$_3$ in DPBS). Primary and secondary antibodies were diluted in blocking buffer and incubated for 2 h at room temperature. Coverslips were mounted using Gelvatol or Prolong Diamond (ThermoFisher Scientific) and imaged with an inverted confocal microscope (Zeiss LSM700). Images were processed with ImageJ/FIJI. For 3D-structured illumination microscopy (SIM) (Fig. 1e), wild-type and knockout FEFs were plated on 1.5-mm coverslips and immunostained as above. Coverslips were mounted with Vectashield (Vectorlabs). 3D-SIM imaging was performed on a Zeiss Elyra PS.1 microscope equipped with a 100×/1.40 NA oil objective. Exciting light was directed through a movable optical grating to generate a fine-striped interference pattern on the same plane. z stacks of 15 optical sections with a step size of 0.1 μm were acquired to generate images in maximum intensity projection. The epitope of the ASPM (216-1) antibody[43], NDNYGLNQDLESES, is located before the TALEN target site. The following antibodies were used at 1:100–1:2,000: centrin (Millipore 20H5), PAR6α (SCBT sc-14405), PAR6α (Abcam ab180159), β-actin (Proteintech 20536-1-AP), ASPM (SCBT sc-98903), ASPM (gift from J. Bond, 216-1), ninein (Biolegend Poly6028) and aPKCζ (SCBT sc-216).

Statistics and reproducibility. All experiments in Fig. 1e, l, m, 2a–i, l–q, 3d, 4a–g were repeated independently three times with similar results. No statistical method was used to predetermine sample size. At least three animals or samples were generally analysed per genotype or age. Two-tailed t-tests were performed for most data using Prism 7, unless otherwise stated. Ferret kits were born at a Mendelian ratio but the genotype of each individual kit was random, which inherently randomized our experiments. To perform blinded experiments, the genotype

of each animal was revealed only after the analysis was completed. In ferrets, sex was undifferentiated up to P21, after which only male ferrets were analysed. In mice, sex was undifferentiated up to P0, after which only male mice were analysed. Figure 1j, k, $n = 3$ male ferrets per genotype of >8 months of age. Individual P values can be found in the Source Data associated with this figure. Figure 1n, box plot elements are maximum, third quartile, median, first quartile and minimum. E35: $n = 17$ $Aspm^{+/+}$ or $Aspm^{+/-}$ ferrets and $n = 10$ $Aspm^{-/-}$ ferrets from three litters (significant differences in brain weight between $Aspm^{+/+}$ or $Aspm^{+/-}$ and $Aspm^{-/-}$ ferrets are indicated: $P = 0.0023$); P0: $n = 9$ $Aspm^{+/+}$ or $Aspm^{+/-}$ ferrets and $n = 6$ $Aspm^{-/-}$ ferrets from one litter ($P = 0.0003$); P21/22 (3 weeks): $n = 8$ $Aspm^{+/+}$ or $Aspm^{+/-}$ ferrets and $n = 3$ $Aspm^{-/-}$ ferrets from two litters ($P = 0.0010$); P41 and older animals (>6 weeks): $n = 7$ $Aspm^{+/+}$ or $Aspm^{+/-}$ ferrets and $n = 7$ $Aspm^{-/-}$ ferrets ($P = 0.0094$). Because brain weight was not found to be significantly different after P41, both adult and P41 animals were combined into a '>6 weeks' group. Ferrets display considerable variability in body weight and brain weight at birth, related to variance in the exact time of birth post-conception and to litter size, which can vary from 3 to 15 kits. Thus, one small litter of three P0 kits, including one wild-type and two $Aspm^{+/-}$ young, which had body weights ~2× of the other P0 litters collected, were excluded from brain weight analysis. Because the y axis is log scale, overlaying each data point as dot plots for $n < 10$ does not indicate the distribution of the data efficiently. Instead, brain weight of individual animals can be found in the Source Data associated with this figure. Figure 1o, using the whole-brain images of coronal sections stained with Nissl or DAPI from $n = 6$ animals per genotype, we manually measured mean cortical thickness of the posterior sigmoid gyrus. No significant difference was found ($P = 0.0843$). Figure 1p, the same animals used for MRI (3 $Aspm^{+/-}$ and 3 $Aspm^{-/-}$ ferrets as described above) were used for body weight analysis. No significant difference was found ($P = 0.4481$). Figure 2j, immunofluorescence images were coded and counted blind to genotype by four individuals, and the four independent counts were then averaged for each brain section. The inter-individual correlation was $r \geq 0.89$. Four to six brain sections were imaged and counted per animal, and $n = 3$ $Aspm^{+/+}$ or $Aspm^{+/-}$ and $n = 4$ $Aspm^{-/-}$ littermate E35 animals were analysed. Figure 3f, $Apod^+$ cells from single-molecule fluorescence in situ hybridization were segmented and counted using ImageJ, in an area of dorsal cortex $400 \times 400\,\mu m^2$ centred on the intermediate zone, in multiple sections per animal, with $n = 4$ $Aspm^{+/+}$ or $Aspm^{+/-}$ ferrets and $n = 4$ $Aspm^{-/-}$ ferrets at E35. Per brain average counts were then compared using a one-tailed t-test.

Reporting summary. Further information on experimental design is available in the Nature Research Reporting Summary linked to this paper.

Code availability. The code used in this study is available from the corresponding author upon reasonable request.

Data availability. scRNA-seq data have been deposited in the Gene Expression Omnibus (GEO) under accession number GSE110010. All other data are included in the paper (Source Data for Figs. 1–3) and in the Supplementary Information.

30. Mashiko, D. et al. Generation of mutant mice by pronuclear injection of circular plasmid expressing Cas9 and single guided RNA. *Sci. Rep.* **3**, 3355 (2013).
31. Li, Z., Sun, X., Chen, J., Leno, G. H. & Engelhardt, J. F. Factors affecting the efficiency of embryo transfer in the domestic ferret (*Mustela putorius furo*). *Theriogenology* **66**, 183–190 (2006).
32. Chahboune, H. et al. Neurodevelopment of C57B/L6 mouse brain assessed by in vivo diffusion tensor imaging. *NMR Biomed.* **20**, 375–382 (2007).
33. Petersen, K. F. et al. The role of skeletal muscle insulin resistance in the pathogenesis of the metabolic syndrome. *Proc. Natl Acad. Sci. USA* **104**, 12587–12594 (2007).
34. Rueckert, D. et al. Nonrigid registration using free-form deformations: application to breast MR images. *IEEE Trans. Med. Imaging* **18**, 712–721 (1999).
35. Papademetris, X., Jackowski, A. P., Schultz, R. T., Staib, L. H. & Duncan, J. S. Integrated intensity and point-feature nonrigid registration. In *International Conference on Medical Image Computing and Computer-Assisted Intervention* Vol. 3216 (eds Barillot, C., et al.) 763–770 (Springer, Berlin, 2001).
36. Sawada, K. & Watanabe, M. Development of cerebral sulci and gyri in ferrets (*Mustela putorius*). *Congenit. Anom. (Kyoto)* **52**, 168–175 (2012).
37. Joshi, A. et al. Unified framework for development, deployment and robust testing of neuroimaging algorithms. *Neuroinformatics* **9**, 69–84 (2011).
38. Rahman, A. S., Parvinjah, S., Hanna, M. A., Helguera, P. R. & Busciglio, J. Cryopreservation of cortical tissue blocks for the generation of highly enriched neuronal cultures. *J. Vis. Exp* **45**, e2384 (2010).
39. Trapnell, C. et al. Differential gene and transcript expression analysis of RNA-seq experiments with TopHat and Cufflinks. *Nat. Protoc* **7**, 562–578 (2012).
40. Dobin, A. et al. STAR: ultrafast universal RNA-seq aligner. *Bioinformatics* **29**, 15–21 (2013).
41. Satija, R., Farrell, J. A., Gennert, D., Schier, A. F. & Regev, A. Spatial reconstruction of single-cell gene expression data. *Nat. Biotechnol.* **33**, 495–502 (2015).
42. Villani, A. C. et al. Single-cell RNA-seq reveals new types of human blood dendritic cells, monocytes, and progenitors. *Science* **356**, eaah4573 (2017).
43. Higgins, J. et al. Human ASPM participates in spindle organisation, spindle orientation and cytokinesis. *BMC Cell Biol* **11**, 85 (2010).
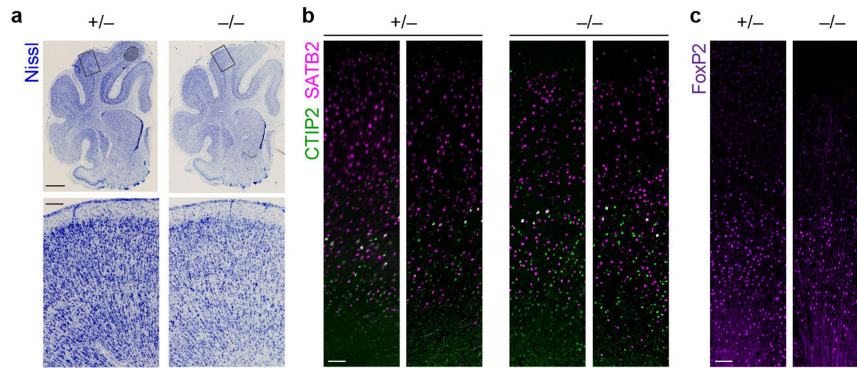
Extended Data Fig. 1 | Cytoarchitecture and neuronal subtype lamination in the cortex of mature *Aspm* knockout ferrets. a, Nissl stains of coronal sections from the brains of P41 littermates, as shown in Fig. 1l, with additional *Aspm*$^{+/-}$ and *Aspm*$^{-/-}$ littermates shown. **b, c**, Brain sections of P41 littermates immunostained for cortical layer-specific projection neurons including SATB2 (layer II–IV), CTIP2 (layer V), and FoxP2 (layer VI). The experiments were repeated independently three times with similar results. Scale bars, 2 mm (**a**, top), 200 μm (**a**, bottom) and 100 μm (**b**, **c**).
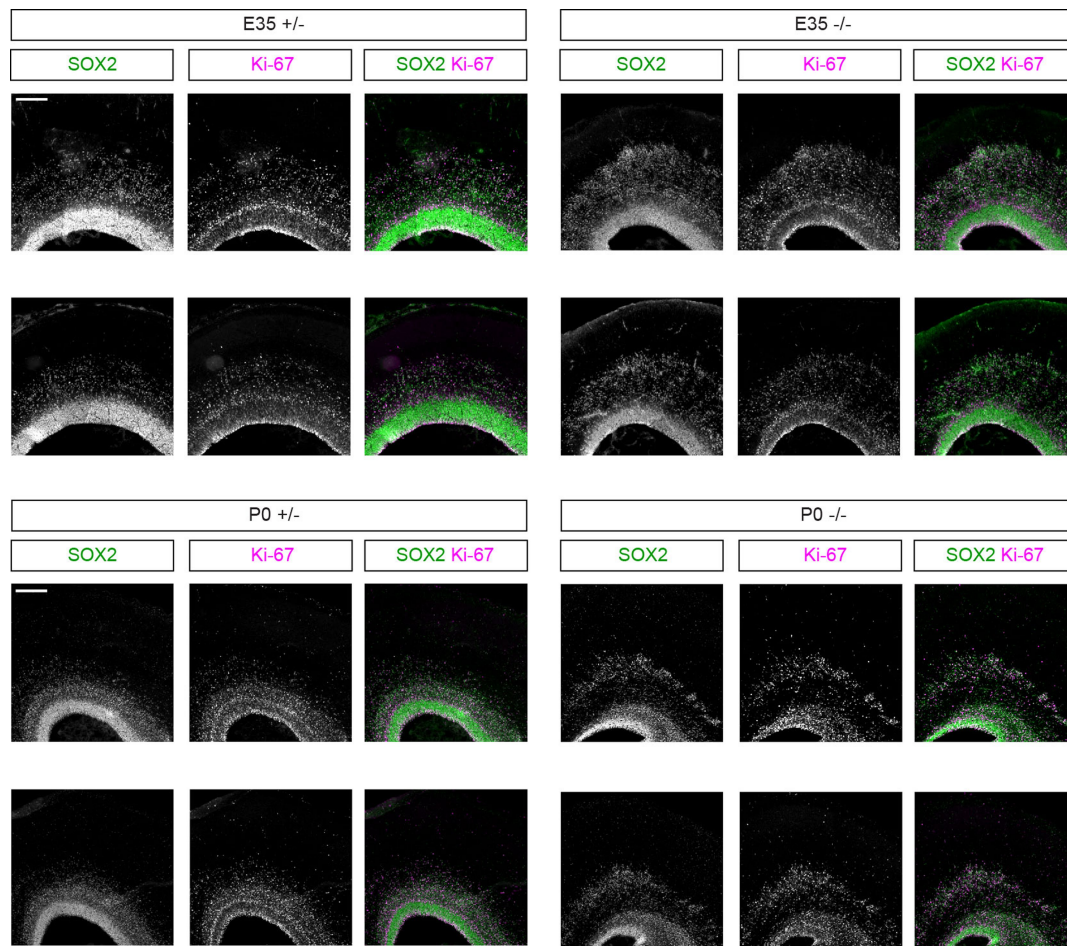
Extended Data Fig. 2 | SOX2 and Ki-67 immunostaining in additional E35 and P0 littermates dorsal cortex. Additional results to Fig. 2e, f. Each set of panels is from the brain of a different littermate, showing the high penetrance of the neural progenitor cell basal displacement phenotype. The experiments were repeated independently three times with similar results. Scale bar, 200 μm.
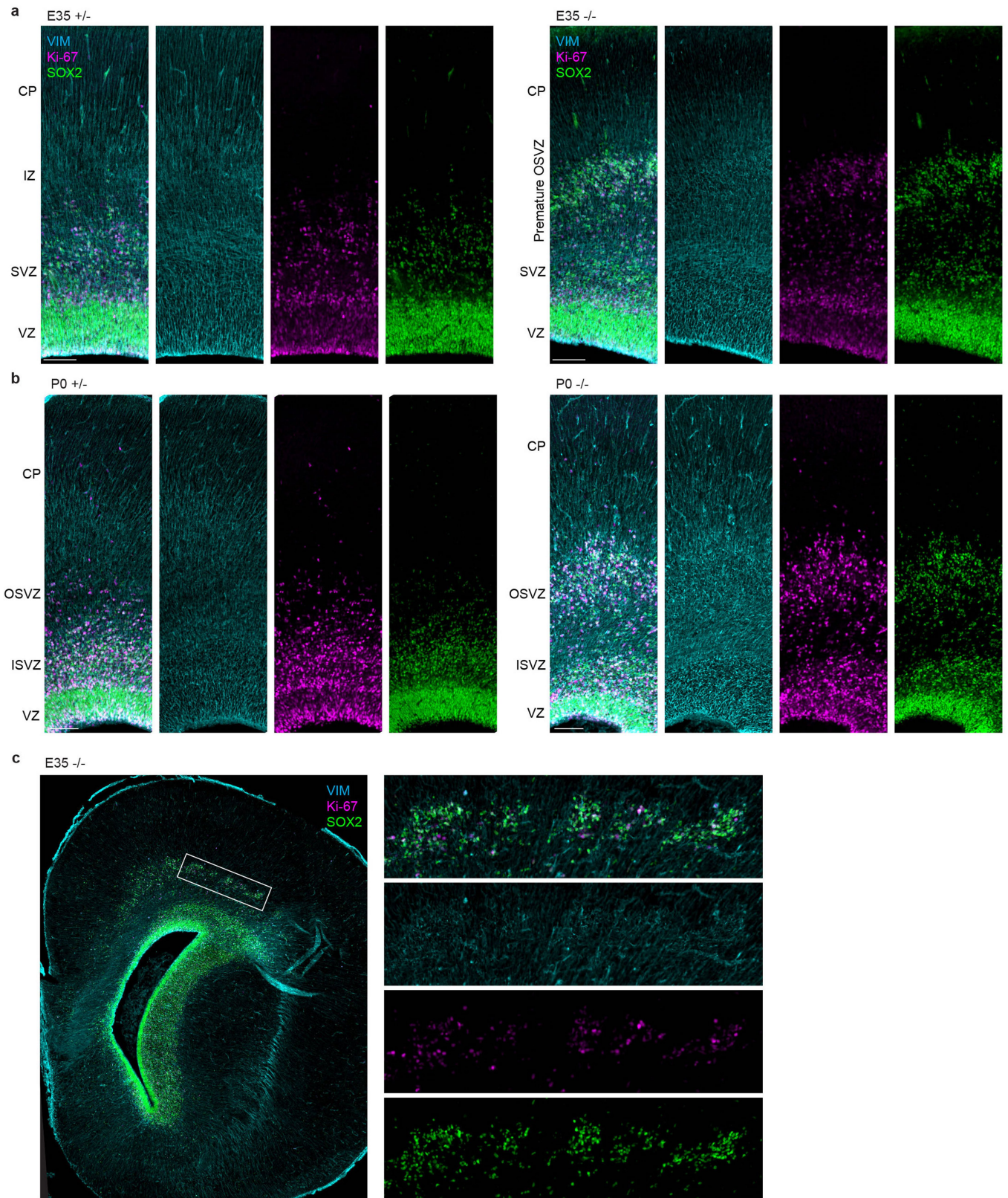
Extended Data Fig. 3 | Displaced progenitors in *Aspm* knockout ferrets have basal fibres. Additional results for Fig. 2h, i. Immunostaining of SOX2, Ki-67 and VIM shows that displaced neural progenitors have basal radial fibres. The experiments were repeated independently three times with similar results. Scale bars, 100 μm.
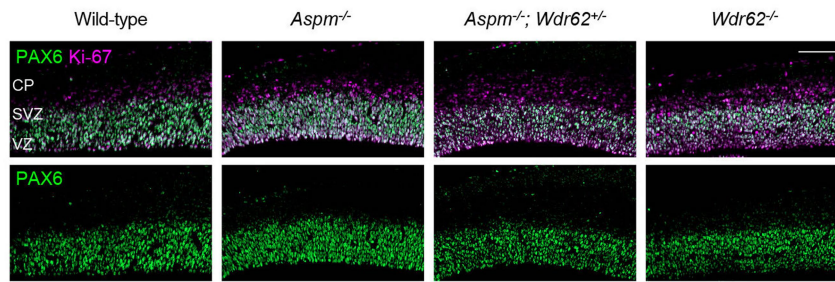
a E14.5 mouse

b E14.5 mouse
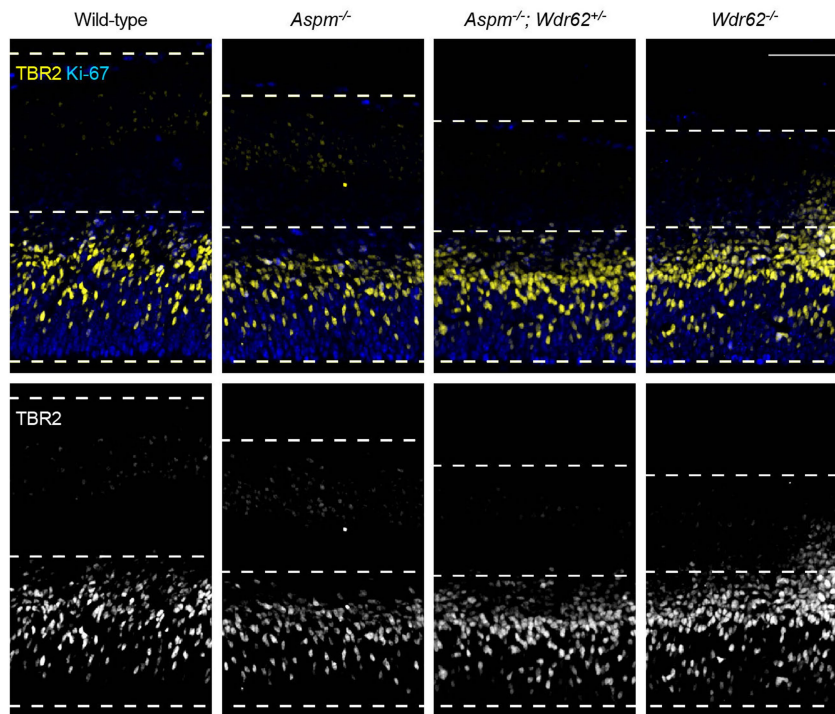
Extended Data Fig. 4 | *Aspm* knockout mice do not demonstrate displaced progenitors in the intermediate zone. a, b, Unlike $Aspm^{-/-}$ ferrets, $Aspm^{-/-}$ mice do not have displaced NPCs in the intermediate zone. However, they show a variable increase in the number of intermediate progenitors (PAX6−Ki-67+ cells in **a** and TBR2+ cells in **b**), which is enhanced by heterozygous, compound mutation in *Wdr62*, a microcephaly gene causing more severe microcephaly[9]. The experiments were repeated independently three times with similar results. Scale bars, 100 μm.
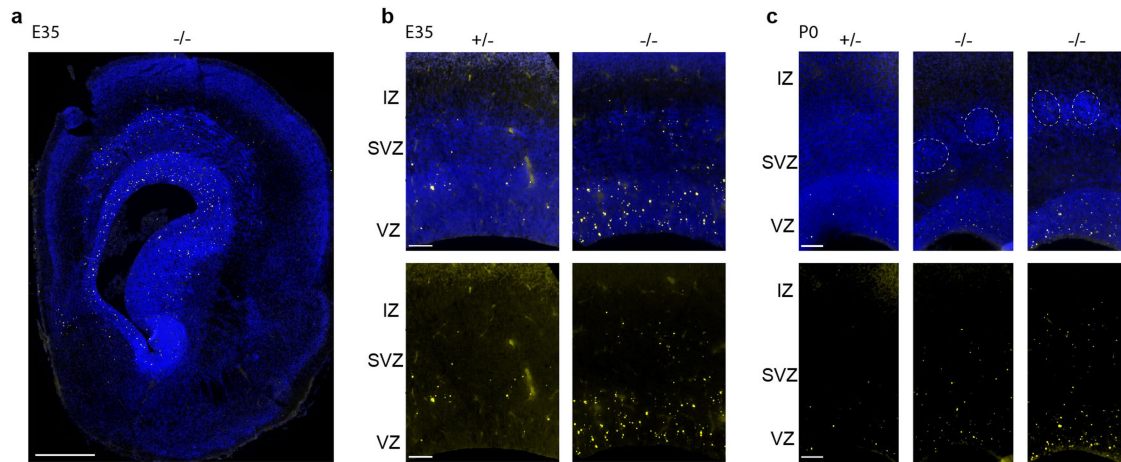
Extended Data Fig. 5 | Modest increase in apoptosis throughout the germinal zones of the *Aspm* knockout telencephalon. Apoptotic cells (yellow) are indicated by enzymatic fluorescence detection of double-stranded DNA damage with DAPI nuclear counterstaining (blue). The experiments were repeated independently three times with similar results. **a**, Whole section. **b**, **c**, Cortical wall columns. Scale bars, 500 μm (**a**) and 100 μm (**b**, **c**).
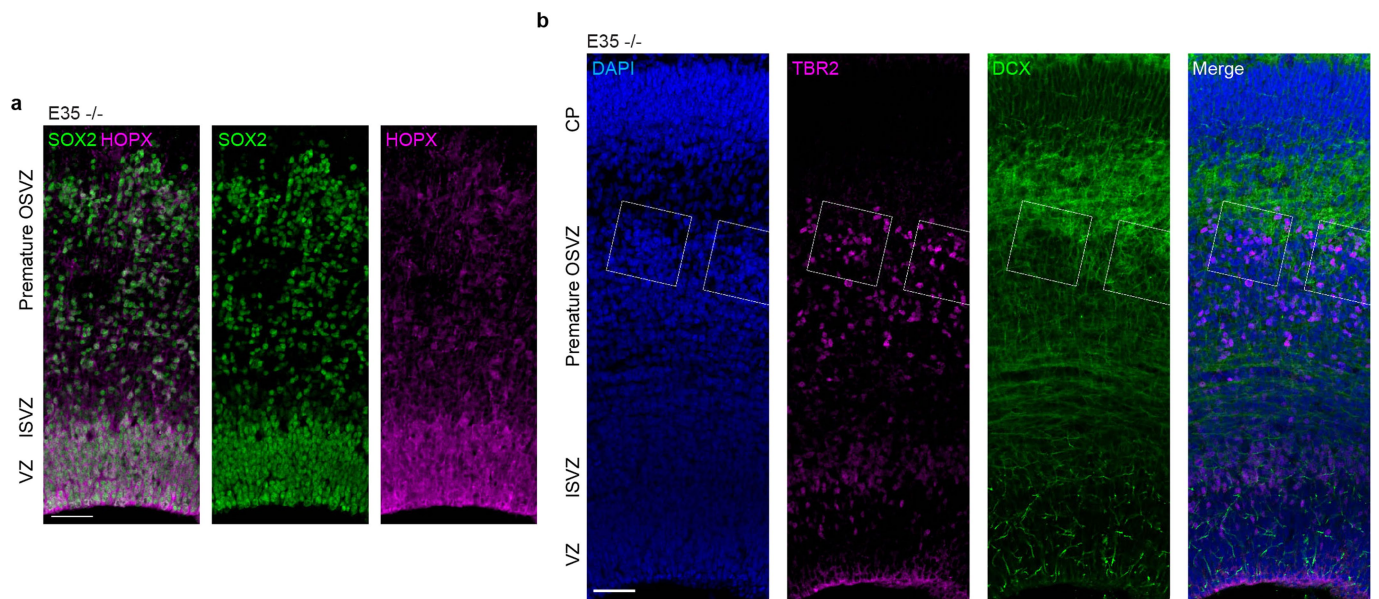
Extended Data Fig. 6 | Additional immunohistochemical analyses of displaced progenitors in the *Aspm* knockout cortex. a, E35 knockout cortex stained for VRG and ORG markers SOX2 and HOPX reveals extensive co-labelling in both the ventricular zone (VZ) and SVZ, including in displaced OSVZ progenitors. **b**, In the E35 knockout OSVZ, clusters of supernumerary displaced neural progenitor cells include numerous TBR2^{+} intermediate progenitors and are surrounded by DCX^{+} newborn neurons, indicating preserved neurogenesis within the precocious OSVZ niche of the *Aspm* knockout cortex. The experiments were repeated independently three times with similar results. Scale bars, 50 μm.
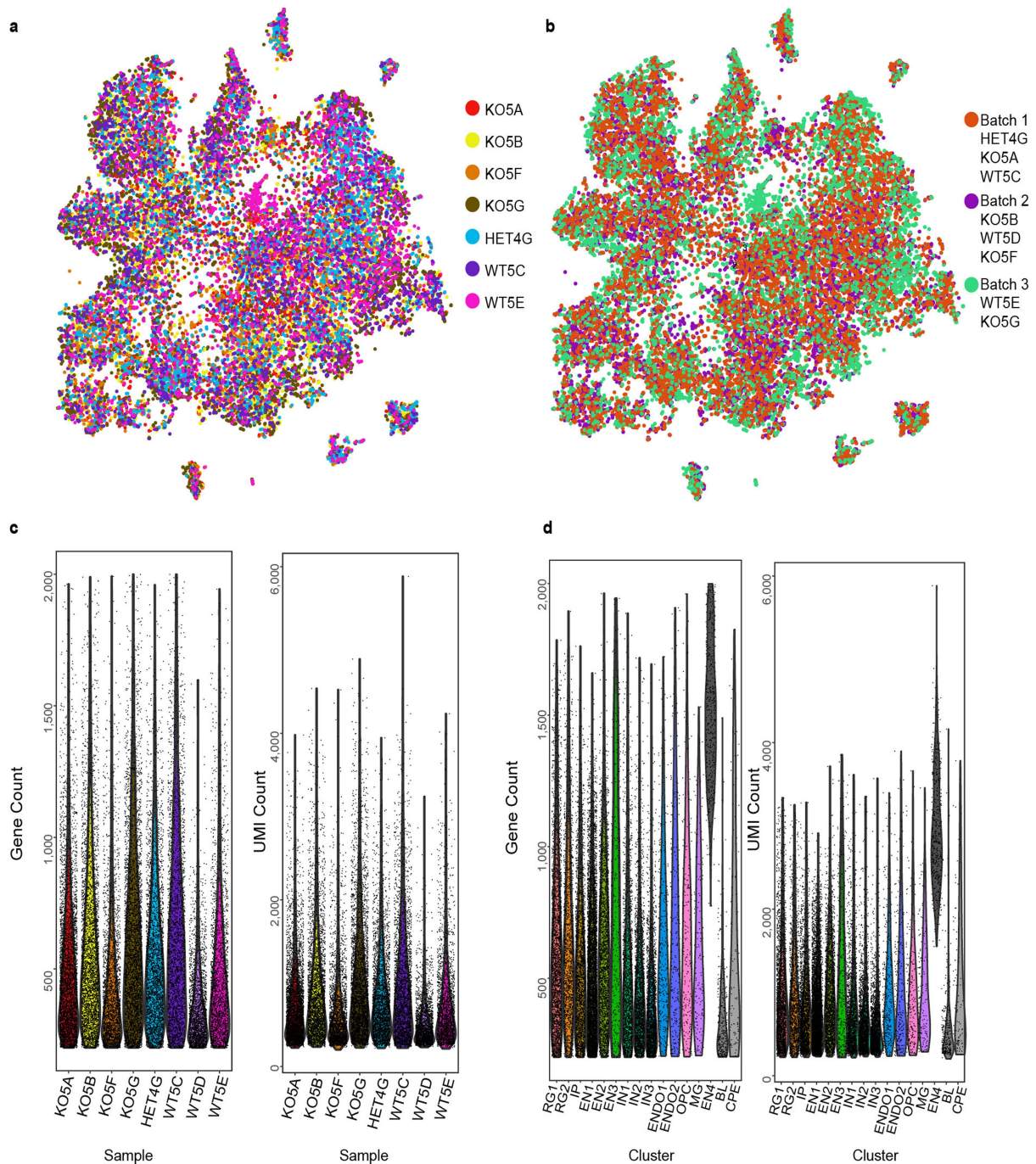
**Extended Data Fig. 7 | scRNA-seq batch, sample and cluster analyses.** **a**, *t*-SNE plot from Fig. 3a with cells coloured by biological replicate (that is, animal). Most clusters include cells from all samples, except for a cluster expressing blood genes and a cluster expressing choroid plexus epithelial cells that are mostly from animal WT5E. These two cell clusters were not included in downstream analyses. HET, heterozygote; KO, knockout; WT, wild type. Numbers and letters indicate litter and animal identification number, respectively. **b**, *t*-SNE plot from Fig. 3a with cells coloured by the batch they were processed in. Clusters are composed of cells from all batches. **c**, Per-cell gene count and UMI count per sample. Each violin plot is one biological replicate and each dot is one cell. Sample WT5D was not included in the analysis due to the lower gene and UMI count compared to other samples as well as the inconsistent clustering compared to other wild-type samples (data not shown). **d**, Per-cell gene count and

UMI count for identified clusters. Each violin plot is one cell cluster and each dot is one cell. The three clusters in grey (EN4, BL, CPE) were not included in downstream analyses. See Methods for details. This scRNA-seq experiment was performed once with $n = 22{,}211$ cells (8,037 cells from two $Aspm^{+/+}$ and one $Aspm^{+/-}$ ferrets and 14,174 cells from four $Aspm^{-/-}$ ferrets). RG1, cycling radial glial progenitors; RG2, interphase radial glial progenitors; IP, intermediate progenitors; EN1, upper-layer excitatory neurons; EN2, deep-layer excitatory neurons; EN3, Cajal–Retzius cells; IN1, immature inhibitory neurons; IN2, SST$^+$ inhibitory neurons; IN3, ventral/inhibitory progenitors; ENDO1, endothelial cells 1; ENDO2, endothelial cells 2; OPC, oligodendrocyte precursors; MG, microglia; EN4, mixed excitatory neuron identity; BL, blood cells; CPE, choroid plexus epithelial cells.
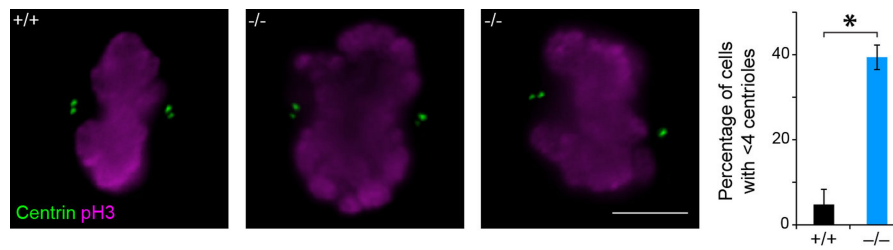
Extended Data Fig. 8 | Loss of *Aspm* disrupts centriole duplication in FEFs. Mitotic *Aspm* knockout FEFs, identified by staining for pH3 and co-stained for the centriolar marker centrin, display a significant loss of centrioles. The percentage of cells with an abnormal number (less than 4) of centrioles is increased eightfold in *Aspm*$^{-/-}$ FEFs compared to *Aspm*$^{+/+}$ FEFs ($n = 100$ cells per genotype for three independent experiments; $P = 0.003$). The experiments were repeated independently three times with similar results. Statistical analysis was performed using a two-tailed *t*-test; data are mean ± s.e.m.

Extended Data Table 1 | Region-specific changes in volume and surface area by loss of *Aspm* in ferrets

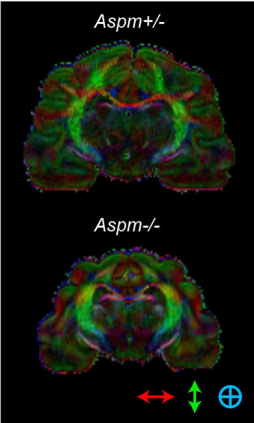**a** Volume (mm^3)

Region	Aspm+/-	Aspm-/-	P-value
Frontal ctx	475.0 ± 58.4	235.0 ± 11.0	0.0156
Corpus callosum	79.3 ± 6.7	40.3 ± 2.3	0.0048
Lateral ctx	666.9 ± 48.4	364.8 ± 33.9	0.0069
Ctx WM	701.4 ± 46.1	402.9 ± 19.0	0.0039
Parietal/occipital ctx	421.6 ± 17.5	256.6 ± 17.5	0.0026
Medial ctx	639.4 ± 58.5	397.3 ± 14.3	0.0159
Hippocampus	319.7 ± 49.8	208.4 ± 18.5	0.0136
Caudate	113.9 ± 13.3	74.8 ± 4.5	0.0478
Putamen	14.3 ± 0.9	10.1 ± 0.4	0.0147
Thalamus	239.7 ± 18.5	172.4 ± 3.4	0.0238
Cerebellum GM	895.0 ± 32.0	650.3 ± 20.7	0.0030
Cerebellum WM	182.5 ± 12.1	141.5 ± 6.2	0.0382
Brainstem GM	263.8 ± 23.1	207.0 ± 8.4	0.0836 (NS)
Brainstem WM	149.8 ± 6.5	121.3 ± 5.7	0.0298
Midbrain WM	43.2 ± 0.6	37.3 ± 0.8	0.0018
Amygdala	23.2 ± 1.1	20.2 ± 1.4	0.1868 (NS)
Midbrain GM	106.0 ± 3.2	101.8 ± 2.6	0.3146 (NS)

b Outer surface area (mm^2)

Region	Aspm+/-	Aspm-/-	P-value
Cerebral ctx (total)	1,225.4 ± 64.1	933.0 ± 47.5	0.0217
Frontal ctx	309.6 ± 18.5	203.5 ± 2.8	0.0048
Lateral ctx	391.9 ± 18.5	301.4 ± 20.5	0.0305
Parietal/occipital ctx	298.4 ± 20.1	217.1 ± 22.7	0.0551 (NS)
Medial ctx	225.5 ± 9.7	211.0 ± 9.5	0.3476 (NS)

c

Aspm+/-

Aspm-/-

d Fractional anisotropy

Region	Aspm+/-	Aspm-/-	P-value
Frontal ctx	0.272 ± 0.002	0.240 ± 0.007	0.0130
Medial ctx	0.255 ± 0.004	0.237 ± 0.009	0.1377 (NS)
Lateral ctx	0.253 ± 0.011	0.252 ± 0.008	0.9198 (NS)
Parietal/occipital ctx	0.267 ± 0.014	0.246 ± 0.014	0.3421 (NS)
Ctx WM	0.431 ± 0.031	0.379 ± 0.018	0.2285 (NS)
Corpus callosum	0.487 ± 0.034	0.434 ± 0.048	0.4170 (NS)
Cingulum	0.415 ± 0.063	0.342 ± 0.053	0.4267 (NS)
Fornix	0.458 ± 0.041	0.435 ± 0.022	0.6542 (NS)
Anterior commisure	0.437 ± 0.069	0.336 ± 0.052	0.3046 (NS)
Optic tract	0.523 ± 0.059	0.435 ± 0.045	0.3013 (NS)
Corticospinal tract	0.550 ± 0.059	0.470 ± 0.041	0.3330 (NS)
Brainstem WM	0.501 ± 0.042	0.423 ± 0.026	0.1925 (NS)
Cerebellum WM	0.454 ± 0.031	0.368 ± 0.033	0.1321 (NS)
Midbrain WM	0.398 ± 0.058	0.338 ± 0.043	0.4496 (NS)
Cerebellum GM	0.301 ± 0.010	0.258 ± 0.007	0.0211
Brainstem GM	0.353 ± 0.011	0.285 ± 0.015	0.0230
Inferior colliculus	0.289 ± 0.001	0.276 ± 0.009	0.2078 (NS)
Superior colliculus	0.270 ± 0.008	0.262 ± 0.008	0.4870 (NS)
Periaqueductal gray	0.273 ± 0.010	0.268 ± 0.003	0.6517 (NS)
Midbrain GM	0.291 ± 0.017	0.270 ± 0.015	0.3974 (NS)
Thalamus	0.286 ± 0.015	0.269 ± 0.003	0.3413 (NS)
Hippocampus	0.270 ± 0.011	0.254 ± 0.002	0.2276 (NS)
Hypothalamus	0.257 ± 0.021	0.225 ± 0.011	0.2533 (NS)
Globus pallidus	0.291 ± 0.020	0.288 ± 0.021	0.9115 (NS)
Putamen	0.285 ± 0.007	0.292 ± 0.023	0.7631 (NS)
Caudate	0.216 ± 0.005	0.221 ± 0.013	0.7161 (NS)
Septum	0.267 ± 0.022	0.245 ± 0.010	0.4183 (NS)
Amygdala	0.206 ± 0.013	0.213 ± 0.019	0.7790 (NS)

a, Multiple brain regions are significantly decreased in volume; the highest reduction was found in the frontal cortex of adult *Aspm*$^{-/-}$ ferrets ($n = 3$ per genotype). Subcortical regions were relatively preserved. **b**, The outer cortical surface is the most reduced in the frontal cortex followed by the lateral cortex. The parietal/occipital cortex is also decreased but the difference was not significant. The medial cortex shows no discernible decrease. **c**, **d**, DTI shows that the orientation of white matter tracts or connectivity is fundamentally unchanged in *Aspm* knockout ferrets except in the frontal cortex, which shows a modest decrease in fractional anisotropy (**d**). The directional map (**c**) shows white matter orientation. Red, green and blue indicate the medial–lateral, superior–inferior, and anterior–posterior components, respectively. Statistical analysis was performed using a two-tailed *t*-test. Data are mean ± s.e.m. NS, not significant.

Extended Data Table 2 | Cluster identifiers of E35 ferret cerebral cortical cells analysed by scRNA-seq

Color	Cluster ID	Top 10 Marker Transcripts	Inferred Cell Type	Cell Count in *Aspm+/-*	Cell Count in *Aspm-/-*	Proportion of *Aspm+/-*	Proportion of *Aspm-/-*	Fold-change in proportion	Empirical P-value
	RG1	TOP2A; HMGB2; CENPF; CENPE; TPX2; XLOC_000183; 2810417H13Rik; SMC4; XLOC_036181; KIF11	Cycling radial glial progenitors	803	1,661	10.5%	12.1%	+15%	0.0002 (FDR<0.01)
	RG2	VIM; HES1; SLC1A3; GDPD2; SFRP1; PON2; PTN; SMPDL3A; NES; PAX6	Interphase radial glial progenitors	495	800	6.5%	5.8%	-10%	0.0696
	IP	NRN1; PTPDC1; TENM4; ELAVL4; ROBO2; FBXW7; IGFBP2; NELL2; PRKX; TTC28	Intermediate progenitors	686	1,603	9.0%	11.7%	+30%	0.0002 (FDR<0.01)
	EN1	SYT4; CSRP2; NEUROD6; NEUROD2; UNC5D; NTM; NSG2; LIMCH1; SORBS2; ISLR2	Upper-layer excitatory neurons	2,203	3,490	28.8%	25.4%	-12%	0.0002 (FDR<0.01)
	EN2	NEFM; FEZF2; NEFL; GRIA2; GUCY1B3; DYNC1I1; ARPP21; NEUROD6; B3GALT2; KCTD12	Deep-layer excitatory neurons	981	1,053	12.8%	7.7%	-40%	0.0002 (FDR<0.01)
	EN3	RELN; LHX1; NDNF; TP73; NHLH2; VSNL1; ENSMPUG00000012124; PLCL1; ENSMPUG00000009767; SEMA6A	Cajal-Retzius cells	103	227	1.3%	1.7%	+23%	0.0704
	IN1	PBX3; MEIS2; XLOC_008478; ENSMPUG00000024751; INA; MAP1B; ATP1B1; XLOC_021005; RUNX1T1; JAKMIP2	Immature inhibitory neurons	591	1,167	7.7%	8.5%	+10%	0.0444
	IN2	SST; XLOC_014564; PDZRN4; NXPH1; NXPH2; SYT1; XLOC_026835; GRIA1; ARX; PDE4DIP	SST interneurons	734	1,568	9.6%	11.4%	+19%	0.0002 (FDR<0.01)
	IN3	XLOC_026835; DLX1; XLOC_026893; CCDC88A; ZNF704; PFN2; EPHA5; XLOC_007250; INA; NR2F1	Ventral/inhibitory progenitors	710	1,521	9.3%	11.1%	+19%	0.0002 (FDR<0.01)
	ENDO1	APOA1; COL4A1; CALD1; SPARC; FN1; IGFBP7; XLOC_010971; ENSMPUG00000012145; LAMA4; MGP	Endothelial cells	122	210	1.6%	1.5%	-4%	0.7418
	ENDO2	SPARCL1; LYZ; PECAM1; IFNAR1; SPARC; IFI27; XLOC_010971; EMB; S100A6; IGFBP7	Endothelial cells	113	150	1.5%	1.1%	-26%	0.0166 (FDR<0.05)
	OPC	APOD; XLOC_017682; SCRG1; DBI; SPARCL1; PDGFRA; SERPINE2; ENSMPUG00000011077; PTPRZ1; LHFPL3	Oligodendrocyte precursors	48	170	0.6%	1.2%	+97%	0.0002 (FDR<0.01)
	MG	ENSMPUG00000001122; C1QC; C3; RGS10; XLOC_039347; CCL8; XLOC_039690; ZFP36; CCL4; SPP1	Microglia	56	105	0.7%	0.8%	+4%	0.7234

The three clusters highlighted in blue represent the largest proportional changes with empirical FDR < 0.01, and are similarly indicated in Fig. 3. Statistical analysis was performed using a two-tailed χ^2 test.

nature research

Corresponding author(s): Christopher A. Walsh & Byoung-Il Bae

Life Sciences Reporting Summary

Nature Research wishes to improve the reproducibility of the work that we publish. This form is intended for publication with all accepted life science papers and provides structure for consistency and transparency in reporting. Every life science submission will use this form; some list items might not apply to an individual manuscript, but all fields must be completed for clarity.

For further information on the points included in this form, see Reporting Life Sciences Research. For further information on Nature Research policies, including our data availability policy, see Authors & Referees and the Editorial Policy Checklist.

Please do not complete any field with "not applicable" or n/a. Refer to the help text for what text to use if an item is not relevant to your study.

For final submission: please carefully check your responses for accuracy; you will not be able to make changes later.

▸ Experimental design

1. **Sample size**

   Describe how sample size was determined.

   No statistical method was employed to predetermine sample size. As is common practice, at least 3 animals or samples were generally analyzed per age/genotype, and individual experiments were repeated at least 3 times to ensure reproducibility (see Figure legends and Methods). Statistical significance was determined using t-tests.

2. **Data exclusions**

   Describe any data exclusions.

   No data were excluded

3. **Replication**

   Describe the measures taken to verify the reproducibility of the experimental findings.

   All the experiments were replicated multiple times.

4. **Randomization**

   Describe how samples/organisms/participants were allocated into experimental groups.

   We bred heterozygous knockout (KO) ferrets (het x het), or a homozygous KO male and a heterozygous female (hom x het). The pups were born at Mendelian ratio but individual pup's genotype was random. This inherently randomized our experiments.

5. **Blinding**

   Describe whether the investigators were blinded to group allocation during data collection and/or analysis.

   Throughout research, the investigators were blinded. The genotype of a sample was revealed only after the analysis was completed.

   Note: all in vivo studies must report how sample size was determined and whether blinding and randomization were used.

6. **Statistical parameters**

   For all figures and tables that use statistical methods, confirm that the following items are present in relevant figure legends (or in the Methods section if additional space is needed).

n/a	Confirmed	
☐	☒	The exact sample size (n) for each experimental group/condition, given as a discrete number and unit of measurement (animals, litters, cultures, etc.)
☐	☒	A description of how samples were collected, noting whether measurements were taken from distinct samples or whether the same sample was measured repeatedly
☐	☒	A statement indicating how many times each experiment was replicated
☐	☒	The statistical test(s) used and whether they are one- or two-sided *Only common tests should be described solely by name; describe more complex techniques in the Methods section.*
☐	☒	A description of any assumptions or corrections, such as an adjustment for multiple comparisons
☐	☒	Test values indicating whether an effect is present *Provide confidence intervals or give results of significance tests (e.g. P values) as exact values whenever appropriate and with effect sizes noted.*
☐	☒	A clear description of statistics including central tendency (e.g. median, mean) and variation (e.g. standard deviation, interquartile range)
☐	☒	Clearly defined error bars in all relevant figure captions (with explicit mention of central tendency and variation)

See the web collection on statistics for biologists for further resources and guidance.

▶ Software

Policy information about availability of computer code

7. Software

Describe the software used to analyze the data in this study.

> The 2017 online versions of EMBOSS Needleall, simple modular architecture research tool (SMART) and Timetree.org for ASPM protein homology and domain analysis; TopHat2 (ver. 2.1.1), Seurat (ver. 1.4.0.5), Cufflinks (ver. 2.2.1), Star (ver. 2.5.2a), Drop-Seq Computational Protocol (ver. 1.0.1), R (ver. 3.3.1), Picard (ver. 1.130 and ver. 1.138), and Samtools (ver. 1.3) for scRNA-seq; BioImage Suite (ver. 3), FreeView (ver. 6), and Matlab (ver. 9) for MRI; Prism (ver. 7) and Excel (ver. 16.9 for Mac) for statistical analysis; ImageJ (ver. 1.46r) for image analysis.

For manuscripts utilizing custom algorithms or software that are central to the paper but not yet described in the published literature, software must be made available to editors and reviewers upon request. We strongly encourage code deposition in a community repository (e.g. GitHub). *Nature Methods* guidance for providing algorithms and software for publication provides further information on this topic.

▶ Materials and reagents

Policy information about availability of materials

8. Materials availability

Indicate whether there are restrictions on availability of unique materials or if these materials are only available for distribution by a third party.

> All the unique materials are available from the authors after an material transfer agreement is completed.

9. Antibodies

Describe the antibodies used and how they were validated for use in the system under study (i.e. assay and species).

For all monoclonal antibodies, the clone numbers were provided. Pax6 (Abcam, ab5790, rabbit polyclonal, immunohistochemistry, 1:500, http://www.abcam.com/pax6-antibody-ab5790.html), Foxp2 (Abcam, ab16046, rabbit polyclonal, immunohistochemistry, 1:500, http://www.abcam.com/foxp2-antibody-ab16046.html); Ctip2 (Abcam, clone 25B6, ab18465, rat monoclonal, immunohistochemistry, 1:500, http://www.abcam.com/ctip2-antibody-25b6-chip-grade-ab18465.html); Satb2 (Bethyl, A301-864A, rabbit polyclonal, immunohistochemistry, 1:500, https://www.bethyl.com/product/A301-864A/SATB2+Antibody); Satb2 (Abcam, clone SATBA4B10, ab51502, mouse monoclonal, immunohistochemistry, 1:200, http://www.abcam.com/satb2-antibody-satba4b10-ab51502.html); Sox2 (Santa Cruz Biotechnology, clone Y-17, sc-17320, goat polyclonal, immunohistochemistry, 1:250, https://www.scbt.com/scbt/product/sox-2-antibody-y-17); Tbr2 (Millipore, AB15894, chicken polyclonal, immunohistochemistry, 1:250, https://www.emdmillipore.com/US/en/product/Anti-Tbr2-Antibody,MM_NF-AB15894); Ki67 (BD Biosciences, clone B56, 550609, mouse monoclonal, immunohistochemistry, 1:2000, http://www.bdbiosciences.com/us/applications/research/intracellular-flow/intracellular-antibodies-and-isotype-controls/anti-rat-antibodies/purified-mouse-anti-ki-67-b56/p/550609); phospho-Vimentin (MBL, clone 4A4, D076-3, mouse monoclonal, immunohistochemistry, 1:1000, https://www.mblintl.com/products/d076-3); Vimentin (Abcam, clone RV202, ab8978, mouse monoclonal, immunohistochemistry, 1:1000, http://www.abcam.com/vimentin-antibody-rv202-ab8978.html), phospho-histone H3 (Millipore, 07-145, rabbit polyclonal, immunohistochemistry, 1:1000, https://www.emdmillipore.com/US/en/product/Anti-phospho-Histone-H3-%28Ser28%29-Antibody,MM_NF-07-145); Hopx (Santa Cruz Biotechnology, sc-30216, rabbit polyclonal, immunohistochemistry, 1:500, https://www.scbt.com/scbt/product/hop-antibody-fl-73); Arl13b (Abcam, clone N295B/66, ab136648, mouse monoclonal, immunohistochemistry, 1:200, http://www.abcam.com/arl13b-antibody-n295b66-ab136648.html); Arl13b (ProteinTech, 17711-1-AP, rabbit polyclonal, immunohistochemistry, 1:500, http://www.ptglab.com/Products/ARL13B-Antibody-17711-1-AP.htm); Neurog2 (R&D, clone 7G4, MAB3314, mouse monoclonal, immunohistochemistry, 1:200, https://www.rndsystems.com/products/human-rat-neurogenin-2-antibody-7g4_mab3314); Doublecortin (Santa Cruz Biotechnology, sc-8066, goat polyclonal, immunohistochemistry, 1:500, https://www.scbt.com/scbt/product/doublecortin-antibody-c-18); Centrin (Millipore, clone 20H5, 04-1624, mouse monoclonal, immunocytochemistry, 1:1000, https://www.emdmillipore.com/US/en/product/Anti-Centrin-Antibody%2C-clone-20H5,MM_NF-04-1624); Par6α (Santa Cruz Biotechnology, sc-14405, goat polyclonal, immunocytochemistry, 1:500, https://www.scbt.com/scbt/product/pard6a-antibody-t-20); Par6α (Abcam, clone EPR12378, ab180159, rabbit monoclonal, western blotting, 1:1000, http://www.abcam.com/par6-antibody-epr12378-n-terminal-ab180159.html); Beta-actin (Proteintech, 20536-1-AP, rabbit polyclonal, western blotting, 1:2000, https://www.ptglab.com/products/ACTB-Antibody-20536-1-AP.htm); ASPM (Santa Cruz Biotechnology, sc-98903, rabbit polyclonal, immunocytochemistry at 1:100, western blotting at 1:500, 1-2 μg for immunoprecipitation, https://www.labome.com/product/Santa-Cruz-Biotechnology/sc-98903.html, discontinued); ASPM (gift from Dr. Jacquelyn Bond, 216-1, rabbit polyclonal, immunocytochemistry, 1:100); Ninein (Biolegend, Poly6028, rabbit polyclonal, immunocytochemistry, 1:1000, https://www.biolegend.com/en-us/products/purified-anti-ninein-antibody-2038); aPKCζ (Santa Cruz Biotechnology, sc-216, goat polyclonal, immunocytochemistry at 1:100, western blotting at 1:500, 1-2 μg for immunoprecipitation, https://www.scbt.com/scbt/product/pkc-zeta-antibody-c-20); γ-tubulin (Sigma-Aldrich, T5326, mouse monoclonal, clone GTU-88, immunocytochemistry, 1:200, immunohistochemistry, 1:250, http://www.sigmaaldrich.com/catalog/product/sigma/t6557?lang=en&region=US)

10. Eukaryotic cell lines

a. State the source of each eukaryotic cell line used.

H4 (ATCC), Hela (ATCC)

b. Describe the method of cell line authentication used.

H4 and Hela cells authenticated by short tandem repeat DNA profiling were obtained directly from ATCC and used within 5 passages.

c. Report whether the cell lines were tested for mycoplasma contamination.

All cell lines were mycoplasma-negative, which was confirmed by two different methods.

d. If any of the cell lines used are listed in the database of commonly misidentified cell lines maintained by ICLAC, provide a scientific rationale for their use.

No commonly misidentified cell lines were used.

▶ Animals and human research participants

Policy information about studies involving animals; when reporting animal research, follow the ARRIVE guidelines

11. Description of research animals

Provide all relevant details on animals and/or animal-derived materials used in the study.

Domestic ferrets (Mustela putorius furo) with disrupted Aspm gene. N = 3-17/age. Age E35 to P785. Sex was undifferentiated up to P21 and ratio was 1:1. After P21, only male ferrets were used.

Aspm KO mice were maintained in C57BL/6 background. Up to P0, sex was undifferentiated and ratio was 1:1. After P0, only male mice were used.

Policy information about studies involving human research participants

12. Description of human research participants

Describe the covariate-relevant population characteristics of the human research participants.

No human research participants.

nature research

Corresponding author(s): Christopher A. Walsh & Byoung-Il Bae

MRI Studies Reporting Summary

Form fields will expand as needed. Please do not leave fields blank.

▶ Experimental design

1. Describe the experimental design.

   Structural MRI and MR diffusion tensor imaging (DTI) of perfused/ fixed ferret brains

2. Specify the number of blocks, trials or experimental units per session and/or subject, and specify the length of each trial or block (if trials are blocked) and interval between trials.

   One volume per sample; typically required about 3 hours of imaging

3. Describe how behavioral performance was measured.

   n/a

▶ Acquisition

4. Imaging

   a. Specify the type(s) of imaging.

   Structural imaging and diffusion tensor imaging (DTI)

   b. Specify the field strength (in Tesla).

   9.4 T

   c. Provide the essential sequence imaging parameters.

   FLASH (Fast Low Angle Shot), TR/TE=100/30 ms, voxel size = 150um isotropic

   d. For diffusion MRI, provide full details of imaging parameters.

   Stejskal and Tanner spin-echo diffusion weighted sequence; diffusion gradient δ = 5 ms; delay Δ = 15 ms; 64 slices; 500 μm thickness; field of view=25.6 mm × 25.6 mm; matrix=128 × 128 resolution; TR = 4s, TE = 30 ms; 4 averages. 15 non-collinear diffusion weighted directions (b=1000 s/mm2) and 1 without diffusion weighting. Tensor eigenvalues and their corresponding eigenvectors were computed, along with fractional anisotropy, at each voxel with BioImage Suite. Images color-coded by the principal direction (eigenvector) of diffusion also using BioImage Suite (http://www.bioimagesuite.org/).

5. State area of acquisition.

   Whole brain scan

▶ Preprocessing

6. Describe the software used for preprocessing.

   Freeview and BioImage Suite

7. Normalization

   a. If data were normalized/standardized, describe the approach(es).

   All data were processed in individual subject space.
   For structural images, intensities were corrected for B1 inhomogeneity correction.

   b. Describe the template used for normalization/ transformation.

   An atlas (Hutchinson, et al. (2017). Population based MRI and DTI templates of the adult ferret brain and tools for voxelwise analysis. NeuroImage, 152, 575–589.) was warped to each individual subject to quantify volumes of interest. However the analysis was performed in individual subject space, i.e. the registration mapped the atlas to the subjects.

8. Describe your procedure for artifact and structured noise removal.

   n/a

9. Define your software and/or method and criteria for volume censoring, and state the extent of such censoring.

   n/a

▶ Statistical modeling & inference

10. Define your model type and settings.

n/a

11. Specify the precise effect tested.

n/a

12. Analysis

a. Specify whether analysis is whole brain or ROI-based.

ROI-based

b. If ROI-based, describe how anatomical locations were determined.

The segmentations from the ATLAS were warped to each subject to compute volumes.

13. State the statistic type for inference.
(See Eklund et al. 2016.)

Volumes for individual ROIs defined by the atlas.

14. Describe the type of correction and how it is obtained for multiple comparisons.

n/a

15. Connectivity

a. For functional and/or effective connectivity, report the measures of dependence used and the model details.

n/a

b. For graph analysis, report the dependent variable and functional connectivity measure.

n/a

16. For multivariate modeling and predictive analysis, specify independent variables, features extraction and dimension reduction, model, training and evaluation metrics.

n/a